THE ASTROPHYSICAL JOURNAL, 463:205–223, 1996 May 20

A CS AND NH_3 SURVEY OF REGIONS WITH H_2O MASER EMISSION

GUILLEM ANGLADA, ROBERT ESTALELLA, AND JOSEFA PASTOR
Departament d'Astronomia i Meteorologia, Universitat de Barcelona, Av. Diagonal 647, E-08028 Barcelona, Spain
LUIS F. RODRÍGUEZ
Instituto de Astronomía, UNAM, Apdo. Postal 70-264, 04510 México, D.F., Mexico
AND
AUBREY D. HASCHICK
Haystack Observatory, Off Route 40, Westford, MA 01886
Received 1995 August 7; accepted 1995 December 6

ABSTRACT

We present CS ($J = 1 \rightarrow 0$) and NH_3 (1, 1) observations toward 172 different star-forming regions (99 observed in both molecules) associated with H_2O maser emission. We make a comparative study between the physical parameters obtained from the CS and NH_3 spectra and their relationship with the H_2O maser emission. We compare the detection rates, line intensities, line widths, and central velocities of the CS and NH_3 emissions. We find a relationship between the velocity range of the H_2O maser emission and its luminosity, the masers with high-velocity components being more luminous than masers without high-velocity components, which suggests that the maser-pumping mechanism is related to kinetic energy dissipated when small maser condensations move through the molecular cloud. We find that both the CS and the NH_3 lines are significantly wider in regions with H_2O masers than in other regions. Furthermore, for the first time, we find evidence that these line widths increase with the H_2O maser luminosity. These results suggest that the presence of H_2O maser emission is intrinsically associated with an increase of the thermal and turbulent energy of the ambient cloud, in agreement with the current models that propose that the H_2O maser emission originates in shocked regions, such as those associated with the outflows from young stellar objects.

Subject headings: ISM: kinematics and dynamics — ISM: molecules — masers — radio lines: ISM — stars: formation

1. INTRODUCTION

Since its discovery (Cheung et al. 1969), H_2O maser emission at 22.235080 GHz ($6_{16} \rightarrow 5_{23}$ transition) from more than 500 nonstellar sources near H II regions or infrared sources associated with molecular clouds has been detected. Genzel & Downes (1977, 1979) showed the close relationship between H_2O maser emission and recent star formation. Dinger & Dickinson (1980) made a catalog containing the interstellar H_2O masers that had been detected up to that time (195 sources). By 1983 the total number of detected H_2O masers had increased by $\sim 50\%$, and Braz & Epchtein (1983) compiled a new catalog with 288 interstellar H_2O masers located in the Galactic plane. Afterward, Cesaroni et al. (1988) published a new catalog, which included both stellar and interstellar H_2O masers (a total of 526 sources), with declination higher than $-30°$. The sources of this catalog were reobserved with the Medicina 32 m telescope (Comoretto et al. 1990), which provided a large sample of H_2O maser spectra taken with the same instrument and in the same epoch. Palagi et al. (1993) associated 262 of these sources with star-forming regions. Brandt et al. (1994) presented an update of the Comoretto et al. (1990) catalog, with 214 new sources (152 of them potentially associated with star-forming regions). Codella et al. (1994, 1995) reported 35 newly detected maser sources north of declination $-30°$ associated with star-forming regions. For declinations below $-30°$ no such complete study has been performed (lists of southern hemisphere H_2O masers can be found in, e.g., Braz & Epchtein 1983; Braz et al. 1989; Scalise, Rodríguez, & Mendoza-Torres 1989).

In addition to the compilation of increasingly more extensive catalogs, an important effort has been made, especially in the last few years, in order to study the excitation mechanism of maser emission and the relationship between H_2O maser emission and other signposts of star formation. In particular, these issues include the stage of the early stellar evolution in which the H_2O maser emission starts, the duration of the maser activity, its relationship with the outflow phenomenon, and the role of shocks in the maser excitation (see, e.g., Henning et al. 1992; Felli, Palagi, & Tofani 1992; Xiang & Turner 1995; Tofani et al. 1995), as well as the relationship with FIR emission, ultracompact H II regions, and high-density gas (see, e.g., Scalise et al. 1989; Wood & Churchwell 1989; Churchwell, Walmsley, & Cesaroni 1990; Palla et al. 1991, 1993; Plume, Jaffe, & Evans 1992; Palagi et al. 1993; Wilking et al. 1994; Persi, Palagi, & Felli 1994; Codella et al. 1994, 1995; Codella & Felli 1995; Zinchenko, Mattila, & Toriseva 1995).

In this paper we report CS ($J = 1 \rightarrow 0$) and NH_3 (J, K) = (1, 1) observations toward a large sample of H_2O maser regions. We observed a total of 172 sources, 107 of which were observed in CS and 164 in NH_3. The main purpose of this work was to study the relationship between the parameters that characterize the high-velocity H_2O maser emission, which originates in very small (~ 10 AU) and very dense (10^7–10^9 cm^{-3}) regions, and those that characterize the molecular emission coming from quiescent, more extended (0.1–1.0 pc) high-density (10^4–10^5 cm^{-3}) regions, traced by the CS and NH_3 emissions. These relationships may provide significant information about the physics of these regions and the interaction of maser condensations

with the surrounding molecular medium. In § 2 we describe our NH_3 and CS observations, in § 3 we present the results obtained in these observations, and in § 4 we analyze and discuss these results: we compare the CS and NH_3 line parameters (§ 4.1), we analyze the statistical properties of our H_2O masers sample (§ 4.2), and we study the relationship between the H_2O maser emission and the ambient dense molecular gas traced by the CS and NH_3 emissions (§ 4.3). In § 5 we give the conclusions of our analysis.

2. OBSERVATIONS

The observations were carried out between 1986 and 1990 with the 37 m radio telescope at Haystack Observatory[1] (Westford, Massachusetts). We observed the emission of the $(J, K) = (1, 1)$ inversion transition of the NH_3 molecule at 23.694496 GHz and the emission of the $J = 1 \rightarrow 0$ rotational transition of the CS molecule at 48.990968 GHz.

Most NH_3 observations were made in 1986 August and September. At the frequency of the observed NH_3 transition the half-power beamwidth of the radio telescope was 1'.4, and the beam efficiency at an elevation of 45° was ~32%. The observations were made using the total power, position-switching mode. We used a cooled K-band maser receiver and a 512 channel digital autocorrelation spectrometer with an effective bandwidth of 13.3 MHz, which gives a velocity coverage of ~168 km s^{-1} at the frequency of 23.7 GHz. The spectra were taken using unity weighting. The calibration was carried out with a noise tube. The system temperature obtained ranged from 100 to 290 K, depending on source elevation and atmospheric conditions. Pointing was checked to be better than ~15″ by observing continuum unresolved sources. All the spectra were corrected for elevation-dependent gain variations and for atmospheric attenuation. After Hanning weighting, the spectral resolution was $\delta V \simeq 0.8$ km s^{-1}. Two additional sources were observed in 1988 February and May (AFGL 5142 and AFGL 5157, Verdes-Montenegro et al. 1989) and another in 1990 February (L1448N), using 1024 channels with an effective bandwidth of 6.67 MHz, giving a velocity coverage of ~84 km s^{-1} and providing a spectral resolution of $\delta V \simeq 0.2$ km s^{-1}.

The CS observations were made in 1987 August and 1988 August. At the frequency of the observed CS transition the half-power beamwidth of the radio telescope was 41″, and the beam efficiency at an elevation of 45° was ~9%. The observations were made using the total power, position-switching mode. We used a cooled K-band maser receiver and a 512 channel digital autocorrelation spectrometer with an effective bandwidth of 13.3 MHz, which gives a velocity coverage of ~82 km s^{-1} at the frequency of 49.0 GHz. The system temperature obtained ranged from 160 to 280 K, depending on source elevation and atmospheric conditions. Calibration of the CS observations was made in a similar way as the NH_3 observations. After Hanning weighting, the spectral resolution was $\delta V \simeq 0.4$ km s^{-1}. For the sources Orion KL-A, NGC 2024, NGC 2071, and NGC 7538S we used 1024 channels, with an effective bandwidth of 6.67 MHz, giving a velocity coverage of ~41 km s^{-1} and providing a spectral resolution of $\delta V \sim 0.1$ km s^{-1}.

We compiled an initial catalog that contained the positions of the interstellar H_2O masers known at the starting epoch of the observations (1986 August). Sources that were not observable from Haystack Observatory, with declination below −38°, were not included. In the catalog, we considered as a single source the masers whose positions were separated by less than 20″, an angular distance significantly smaller than the resolution of our telescope. Masers with an angular separation greater than 20″ were considered as different sources. The projected physical separation in all these cases was larger than 1 pc, except for Mon R2(1) and Mon R2(2). Even for the case of these two masers, which are separated 1'.2 (corresponding to only 0.27 pc), it seems adequate to consider them as two different sources since they are probably associated with different excitation sources (Torrelles et al. 1990). The resulting initial catalog of H_2O maser sources contained 204 positions and is given in Table 1. After a total observing time of about 500 hr devoted to this program, we completed observations of 107 sources in CS and 164 in NH_3. We observed, at least in one of these two molecules, a total of 172 sources (80% of the initial catalog), 99 out of them being observed in both molecules. In some of the sources observed in NH_3, four additional positions 1'.2 apart from the nominal position given in Table 1 were also observed.

In Table 1 we also give, for the observed sources, the central velocity of the observed bandwidth, V, the 1 σ sensitivity per spectral channel, and whether the emission was detected or not. The detection criterion takes into account the spectral line width as compared with the spectral resolution. Therefore, we defined the signal-to-noise ratio (SNR) of a spectrum as SNR $= (T_A^*/\sigma)(\Delta V/\delta V)^{1/2}$, where T_A^* is the line intensity, σ is the sensitivity, ΔV is the line width, and δV is the spectral resolution. We considered as detections the spectra with SNR > 3, though detections with SNR < 5 were considered as questionable (indicated with a question mark in Table 1).

3. OBSERVATIONAL RESULTS

In Table 2 we present the line parameters obtained from Gaussian fits to the spectra, after having subtracted a polynomial baseline. For the NH_3 lines, the parameters in Table 2 correspond to the main line. We give, for each region, the antenna temperature corrected for elevation-dependent gain variations and for atmospheric attenuation, T_A^*, the central velocity of the line, V, and the line width (full width at half-maximum intensity), ΔV, with their respective formal errors. The velocities in the spectra have been corrected for the errors introduced by the Haystack Observatory autocorrelator ($\lesssim 0.2$ km s^{-1}), according to the specifications given by Ball & Haschick (1988), and Ball (1989).

Of the 172 sources observed in at least one of the two molecules, 95% were observed in NH_3, while 62% were observed in CS (Table 3). We detected NH_3 in 58% of the H_2O masers observed. Apparently the CS detection rate was higher, 72%, but it must be noted that we preferentially observed in CS those sources that had already been detected in NH_3. On the other hand, a direct comparison is difficult because of the different sensitivities in the observations. In summary, 106 sources of 172 (62%) were detected in at least one of the two molecules, which indicates a remarkable degree of association with the H_2O maser emission. Plume et al. (1992), from a survey of CS ($J = 7 \rightarrow 6$) in regions of star formation traced by the presence of H_2O masers, found a very similar detection rate

[1] Radio astronomy at Haystack Observatory of the Northeast Radio Observatory Corporation is supported by the National Science Foundation.

TABLE 1

INITIAL CATALOG OF SOURCES WITH H_2O MASER EMISSION[a]

REGION	α(1950)	δ(1950)	REFERENCES	V (km s^{-1})	CS σ (K)	CS Detected	NH_3 σ (K)	NH_3 Detected	OTHER NAMES OF THE REGION
Lk Hα 198	00^{h}08^{m}43^s.2	+58°33′41″.0	1	15.0	0.156	No	...	...	
S184	00 49 29.2	+56 17 37.0	2	−32.0	0.103	Yes	0.032	Yes	NGC 281
W3 (1)	02 21 40.8	+61 53 26.0	3	−49.0	0.090	No	0.023	Yes	
W3 (2A+2B)	02 21 53.2	+61 52 20.0	3	−35.0	0.044	Yes	0.020	No	
W3 (3)	02 22 06.1	+61 50 40.0	3	−38.0	0.117	Yes	0.019	Yes	
W3 (OH)	02 23 17.3	+61 38 57.7	3	−48.0	0.052	Yes	0.035	Yes	
S201	02 59 22.4	+60 16 12.0	4	−33.0	0.135	No	...	...	
L1448N	03 22 30.8	+30 34 59.0	5	4.4	...	...	0.046	Yes	IRAS 03225+3034
GL 490	03 23 39.3	+58 36 35.0	6	−13.0	0.164	Yes	...	...	
HH 7–11(B)	03 25 56.6	+31 05 19.0	7	6.0	0.100	Yes	0.058	Yes	
HH 7–11(A)	03 25 58.2	+31 05 44.0	8	...	...	...	...	...	
HH 7–11(C)	03 26 05.0	+31 03 40.0	8	...	...	...	...	...	
T Tauri	04 19 04.2	+19 25 05.0	3	1.0	0.048	No	0.016	No	
AFGL 5142	05 27 27.6	+33 45 37.0	9	0.0	...	...	0.048	Yes	
Orion KL-A	05 32 46.7	−05 24 28.0	3	8.0	0.337	Yes	0.042	Yes	
OMC 2 (2)	05 32 58.0	−05 07 25.0	10	10.0	0.059	Yes	0.033	Yes	
OMC 2 (1)	05 32 59.9	−05 11 29.0	2	12.0	0.069	Yes	0.084	Yes	
HH 1	05 33 54.9	−06 47 02.0	11	7.0	0.082	Yes	0.043	Yes	
AFGL 5157	05 34 35.7	+31 58 24.0	9	−17.7	...	...	0.015	Yes	
GGD 4	05 37 21.8	+23 49 24.0	12	−2.0	0.155	Yes	0.023	Yes	
S235	05 37 31.8	+35 40 18.0	3	−15.0	0.197	Yes	0.026	Yes	GGD 5–6
NGC 2024	05 39 13.7	−01 57 30.0	3	10.0	0.203	Yes	0.028	Yes	Orion B
HH 19–27	05 43 57.5	−00 03 40.0	11	25.0	0.067	Yes	0.019	Yes	NGC 2068
NGC 2071	05 44 31.3	+00 20 48.0	2	11.0	0.199	Yes	0.019	Yes	OH 205.1−14.1
MWC 789	05 59 05.5	+16 31 10.0	1	...	...	...	...	...	
Mon R2 (1)	06 05 17.0	−06 22 40.0	3	5.0	0.082	Yes	0.031	Yes	NGC 2070
Mon R2 (2)	06 05 21.7	−06 22 35.0	3	12.0	0.280	Yes	0.030	Yes	NGC 2070
S252A	06 05 35.5	+20 30 31.0	13	8.0	0.059	Yes	0.018	No	NGC 2075
S252A3	06 05 36.6	+20 39 34.0	14	9.0	0.065	Yes	0.021	Yes	NGC 2075
G188.94+0.89	06 05 53.7	+21 39 09.0	15	−5.0	0.054	Yes	0.027	Yes	
GGD 12–15	06 08 25.7	−06 10 49.5	12	11.0	0.062	Yes	0.031	Yes	
S255/257	06 09 58.2	+18 00 17.0	3	8.0	0.093	Yes	0.043	Yes	
GGD 16–17	06 10 23.0	−06 12 55.0	12	8.0	...	...	0.099	Yes?	
S269	06 11 46.3	+13 50 31.0	3	18.0	0.149	No	0.028	No	
NGC 2264	06 38 25.2	+09 32 12.0	3	10.0	0.058	Yes	0.029	Yes	
GL 1074	07 05 28.5	−10 39 18.0	16	43.0	0.085	Yes	0.027	No	
HHL 50	07 22 33.4	−24 28 58.0	17	25.0	0.175	Yes	0.025	Yes	
OH 0739−14	07 39 58.9	−14 35 38.0	3	31.0	...	...	0.018	No	
G349.09+0.11	17 12 58.4	−37 56 21.0	18	...	...	...	...	...	
G350.01+0.43	17 14 23.1	−37 00 21.0	18	...	...	...	...	...	
G350.10+0.09	17 16 01.0	−37 07 30.0	18	...	...	...	...	...	
NGC 6334B	17 16 34.5	−35 54 44.0	18	...	...	...	...	...	
GGD 25	17 16 56.5	−35 51 57.9	19	...	...	...	...	...	NGC 6334C
NGC 6334D	17 17 20.3	−35 45 48.0	20	...	...	...	...	...	
NGC 6334A	17 17 32.5	−35 44 13.0	18	...	...	...	...	...	
NGC 6334E	17 17 35.1	−35 42 16.0	20	...	...	...	...	...	
G351.58−0.36	17 22 04.2	−36 10 11.0	18	...	...	...	...	...	
G351.77−0.54	17 23 20.9	−36 06 53.0	18	...	...	...	...	...	
G353.46+0.55	17 23 34.2	−34 06 38.0	18	−52.0	0.397	No	0.067	No	
G352.52−0.16	17 23 51.2	−35 17 03.0	18	−46.0	...	...	0.075	No	
G354.61+0.47	17 27 00.6	−33 11 47.0	18	−11.0	0.329	No	0.070	Yes[a]	
G353.41−0.36	17 27 06.5	−34 39 41.0	15	−14.0	...	...	0.240	Yes[b]	
G355.34+0.14	17 30 14.0	−32 46 07.0	18	10.0	...	...	0.293	No	
G356.64−0.33	17 35 26.1	−31 56 00.0	15	−10.0	0.351	No	0.170	Yes[b]	
G358.23+0.11	17 37 41.7	−30 21 17.0	18	...	...	...	...	...	
G358.67−0.05	17 39 23.5	−30 04 30.0	18	...	...	...	...	...	
G359.14+0.03	17 40 15.5	−29 38 08.0	18	...	...	...	...	...	
G359.43−0.11	17 41 29.8	−29 27 13.0	18	...	...	...	...	...	
G359.62−0.25	17 42 30.0	−29 22 25.0	18	...	...	...	...	...	
G0.37+0.04	17 43 11.0	−28 34 40.0	18	39.0	0.204	No	0.134	No	
Sgr B2N	17 44 10.2	−28 21 16.5	3	...	...	...	...	...	
Sgr B2 Main	17 44 10.4	−28 22 00.0	3	26.0	0.262	No	0.243	No	
G359.97−0.46	17 44 10.4	−29 11 03.0	18	21.0	0.233	Yes	0.135	Yes?	
Sgr B2S	17 44 10.6	−28 22 39.0	3	...	...	...	...	...	
RCW 142	17 47 03.4	−28 53 39.0	3	16.0	0.234	Yes	0.119	Yes	
G2.14+0.01	17 47 28.3	−27 05 12.0	18	62.0	0.251	No	0.082	No	
G3.91−0.01	17 51 35.6	−25 34 19.0	21	...	...	...	...	...	
W28A2	17 57 26.8	−24 03 54.0	3	14.0	0.181	Yes	0.130	Yes	G5.89−0.39
G7.47+0.06	17 59 11.7	−22 28 13.0	3	−16.0	...	...	0.085	No	
G8.14+0.22	18 00 00.2	−21 48 29.0	3	...	...	...	...	...	
G9.62+0.19	18 03 16.0	−20 32 01.0	2	6.0	...	...	0.094	No	

TABLE 1—*Continued*

Region	α(1950)	δ(1950)	References	V (km s^{-1})	CS σ (K)	CS Detected	NH_3 σ (K)	NH_3 Detected	Other Names of the Region
G8.67−0.36	18 03 18.6	−21 37 59.0	2	35.0	...	...	0.121	No	
W31 (1)	18 05 40.5	−19 52 23.0	3	...	...	...	...	...	
G11.03+0.06	18 06 42.2	−19 21 56.0	2	...	...	...	...	...	
W31 (2)	18 07 30.3	−19 56 38.0	3	−1.0	0.161	Yes	0.102	Yes	
G12.42+0.50	18 07 56.4	−17 56 37.0	22	10.0	...	...	0.056	No	
G12.89+0.49	18 08 56.3	−17 32 16.0	22	32.0	...	...	0.078	No	
G11.90−0.14	18 09 15.2	−18 42 25.0	21	40.0	...	...	0.066	No	
G12.76+0.33	18 09 15.6	−17 43 35.0	22	22.0	0.153	Yes	0.063	Yes[b]	S40
G12.21−0.10	18 09 43.5	−18 25 05.5	3	7.0	...	...	0.081	Yes	
G12.21−0.12	18 09 48.5	−18 25 25.0	3	25.0	...	...	0.080	Yes	
W33B	18 10 58.9	−18 02 39.0	3	58.0	0.535	No	0.105	Yes	
G13.19+0.04	18 11 11.5	−17 29 13.0	3	−2.0	0.209	No	0.097	Yes[b]	
G13.87+0.28	18 11 41.5	−16 46 34.0	3	−21.0	...	...	0.059	No	
W33A	18 11 44.0	−17 53 08.5	3	40.0	0.212	Yes	...	...	
G14.11+0.09	18 12 52.6	−16 39 59.0	22	8.0	...	...	0.083	No	
G14.17−0.06	18 13 32.9	−16 40 43.0	15	61.0	...	...	0.051	No	
G14.49+0.01	18 13 55.5	−16 21 46.0	22	38.0	0.095	No	0.067	No	
G12.43−1.12	18 13 56.1	−18 42 57.0	22	...	...	...	...	...	S39
G14.60+0.02	18 14 08.1	−16 15 46.0	3	...	...	...	...	...	
G14.45−0.11	18 14 16.4	−16 27 20.0	22	37.0	0.224	No	0.103	Yes[b]	
G13.66−0.60	18 14 30.3	−17 23 22.0	22	48.0	0.158	Yes?	0.054	Yes	
G14.23−0.51	18 15 18.8	−16 50 47.0	22	25.0	0.131	Yes	0.083	Yes	
M16 (1)	18 15 19.4	−13 46 30.0	16	−65.0	...	...	0.063	No	
W37	18 16 00.0	−13 48 00.0	23	25.0	0.089	Yes?	0.050	No	
G14.33−0.64	18 16 00.8	−16 49 06.0	22	23.0	0.132	Yes	0.105	Yes	
GGD 27–28	18 16 14.6	−20 48 41.0	12	−74.0	...	...	0.042	No	
G14.63−0.58	18 16 21.2	−16 31 24.0	22	26.0	0.147	Yes	0.082	Yes	
M16 (2)	18 16 33.8	−13 42 24.0	16	18.0	...	...	0.030	No	
M17 (1)	18 17 30.0	−16 16 03.0	3	4.0	...	...	0.055	Yes[b]	
M17 (2+3)	18 17 30.3	−16 13 06.0	3	19.0	0.230	Yes	0.047	Yes[b]	
M17 (4)	18 17 37.0	−16 03 40.0	10	21.0	...	...	0.057	No	
G16.58−0.05	18 18 17.7	−14 33 19.0	21	63.0	0.197	No	0.026	Yes[b]	
G16.61−0.05	18 18 21.3	−14 32 11.0	21	60.0	0.095	No	0.021	Yes[b]	
GL 2132	18 20 27.9	−13 44 22.0	14	40.0	...	...	0.030	No	
G19.61−0.13	18 24 28.4	−11 55 39.0	24	50.0	0.104	Yes	0.156	No	
G19.60−0.23	18 24 50.1	−11 58 22.0	3	21.0	0.166	No	0.067	Yes?	
G20.08−0.13	18 25 22.6	−11 30 45.0	24	37.0	...	...	0.044	No	
G20.73−0.05	18 26 18.3	−10 54 15.0	24	...	...	...	...	...	
G20.78−0.05	18 26 24.3	−10 51 35.0	24	59.0	...	...	0.104	Yes?	
G21.04−0.06	18 26 56.9	−10 37 49.0	24	35.0	...	...	0.058	No	
GGD 29	18 27 19.2	+01 13 06.0	12	8.0	0.077	Yes	0.057	Yes	Serpens
G21.88+0.02	18 28 16.1	−09 51 01.0	24	30.0	...	...	0.039	No	RCW 169
G22.36+0.07	18 28 59.6	−09 24 31.0	24	89.0	...	...	0.030	Yes?[b]	
G21.37−0.61	18 29 33.1	−10 35 53.0	2	53.0	0.102	No	0.031	Yes?[b]	
G23.95+0.15	18 31 40.8	−07 57 17.0	3	82.0	0.086	Yes	0.031	Yes[b]	
G23.44−0.18	18 31 55.6	−08 33 54.0	21	...	...	...	...	...	
G23.01−0.41	18 31 56.2	−09 03 04.0	21	80.0	0.067	Yes	0.065	Yes	
G24.49−0.04	18 33 22.8	−07 33 54.0	2	116.0	0.076	Yes	0.045	Yes	
G24.29−0.15	18 33 25.4	−07 47 40.0	2	105.0	0.088	No	0.032	No	
G24.79+0.08	18 33 30.3	−07 14 42.0	2	110.0	0.112	Yes	0.040	Yes[b]	W42
IRAS 18385−0512	18 38 32.3	−05 12 00.0	26	17.0	0.177	No	...	...	Scutum
G28.86+0.07	18 41 07.9	−03 38 41.0	2	100.0	0.100	Yes	0.080	No	
IRC +10374	18 41 18.4	+13 54 19.0	4	−4.0	0.098	No	0.040	No	
G29.98+0.10	18 43 04.3	−02 38 20.0	24	...	...	...	...	...	
W43S	18 43 26.7	−02 42 40.0	3	100.0	...	...	0.111	Yes?	
G29.91−0.05	18 43 29.1	−02 45 42.0	24	31.0	...	...	0.051	No	
G30.67+0.10	18 44 21.2	−02 01 15.0	24	−52.0	...	...	0.039	No	
G30.23−0.14	18 44 25.0	−02 31 20.0	24	3.0	...	...	0.045	No	
G30.88+0.13	18 44 38.7	−01 49 40.0	24	40.0	...	...	0.035	No	
G30.90+0.10	18 44 46.7	−01 49 05.0	24	...	...	...	...	...	
G30.96+0.08	18 44 57.5	−01 46 19.0	24	39.0	...	...	0.035	No	
G31.41+0.31	18 44 59.0	−01 16 07.0	3	101.0	0.114	Yes	0.036	Yes[a]	
W43 Main (1)	18 45 02.8	−02 00 45.0	3	90.0	...	...	0.057	No	
W43 Main (2)	18 45 02.8	−02 01 50.0	3	51.0	...	...	0.082	Yes[a]	
W43 OH1612	18 45 05.6	−01 48 39.0	3	35.0	...	...	0.045	No	
G31.06+0.09	18 45 06.1	−01 40 48.0	24	...	...	...	...	...	
W43 Main (3)	18 45 11.0	−01 57 57.0	3	103.0	0.071	Yes	0.044	Yes[a]	
G30.80−0.13	18 45 23.5	−02 00 39.0	24	97.0	0.124	No	0.093	No	
W43 Main (4)	18 45 33.1	−02 00 21.0	3	97.0	...	...	0.037	Yes?[a]	
G31.00−0.08	18 45 34.9	−01 48 35.0	24	74.0	...	...	0.029	No	
G31.29+0.07	18 45 36.8	−01 29 12.0	24	106.0	0.095	Yes	0.063	Yes	
G31.25−0.11	18 46 10.5	−01 36 32.0	21	17.0	...	...	0.030	Yes[b]	

TABLE 1—*Continued*

Region	α(1950)	δ(1950)	References	V (km s^{-1})	CS σ (K)	CS Detected	NH_3 σ (K)	NH_3 Detected	Other Names of the Region
G31.13−0.22	18 46 20.7	−01 45 24.0	1	−35.0	...	...	0.056	No	
G31.21−0.18	18 46 20.7	−01 40 10.0	15	−39.0	...	...	0.078	No	
G31.40−0.26	18 46 57.5	−01 32 33.0	3	89.0	...	...	0.117	No	
G32.15+0.13	18 46 57.7	−00 41 30.0	2	93.0	0.085	Yes	0.066	Yes	
G32.04+0.06	18 47 02.0	−00 49 19.0	24	92.0	0.107	Yes	0.083	Yes	
G32.10−0.08	18 47 36.8	−00 49 53.0	24	46.0	...	...	0.069	Yes?	
G32.80+0.19[c]	18 47 57.4	−00 05 12.0	3	23.0	...	...	0.055	No	
G32.74−0.08[d]	18 48 47.9	−00 15 46.0	24	36.0	...	...	0.056	Yes	
G33.13−0.09	18 49 34.0	+00 04 30.0	3	75.0	...	...	0.059	No	
G33.91+0.11	18 50 16.3	+00 51 45.0	3	109.0	0.118	Yes	0.066	Yes	
W44	18 50 46.4	+01 11 10.0	3	58.0	0.161	Yes	0.076	Yes	
G33.81−0.19	18 51 09.0	+00 37 59.0	2	38.0	...	...	0.059	No	
G35.03+0.3	18 51 29.5	+01 57 43.0	21	67.0	0.134	Yes	0.062	Yes?	
S76W	18 53 34.0	+07 49 45.0	4	4.0	...	...	0.053	Yes	
S76E	18 53 47.0	+07 49 26.0	4	31.0	0.088	Yes	0.040	Yes	
G35.58−0.03	18 53 51.1	+02 16 27.0	3	58.0	...	...	0.066	No	
G35.20−0.74	18 55 40.8	+01 36 30.0	15	33.0	0.224	Yes	0.093	Yes	
W48	18 59 12.8	+01 09 13.0	3	46.0	0.066	Yes	0.122	Yes?	
G40.62−0.14	19 03 34.9	+06 41 55.0	27	35.0	0.082	Yes	0.096	Yes?	
W49N	19 07 49.8	+09 01 17.0	3	10.0	...	...	0.131	No	
W49S	19 07 58.2	+09 00 03.0	3	10.0	...	...	0.041	No	
G43.80−0.12	19 09 31.2	+09 30 51.0	3	41.0	...	...	0.056	No	
G45.10+0.12	19 11 00.3	+10 45 42.0	3	64.0	...	...	0.053	No	
K47	19 11 46.0	+11 07 03.0	3	45.0	...	...	0.090	No	
G45.49+0.13	19 11 50.0	+11 07 47.0	2	63.0	0.075	Yes	0.101	No	
G45.44+0.07	19 11 56.8	+11 03 33.0	3	58.0	0.067	Yes	0.055	No	
G48.61+0.02	19 18 13.1	+13 49 43.5	3	28.0	...	...	0.048	No	
W51W	19 20 53.3	+14 20 47.0	3	52.0	...	...	0.088	No	
W51N	19 21 22.3	+14 25 19.0	3	33.0	...	...	0.084	No	
W51 Main/S	19 21 26.3	+14 24 30.0	3	56.0	0.059	Yes	0.042	Yes	
S87	19 44 12.9	+24 28 27.0	4	30.0	0.084	Yes	0.093	Yes	
S88 B	19 44 41.0	+25 05 02.0	8	7.0	...	...	0.022	No	
K3-50	19 59 50.1	+33 24 17.0	3	−19.0	...	...	0.113	Yes?	
ON 3	19 59 58.4	+33 25 47.0	3	−19.0	0.062	Yes	0.061	No	W58
ON 1	20 08 09.8	+31 22 44.0	3	13.0	0.058	Yes	0.054	Yes	Cygnus 1
ON 2S	20 19 48.9	+37 15 52.0	3	−12.0	0.064	Yes	0.055	Yes	Cygnus 2 S
ON 2N	20 19 51.6	+37 17 00.0	3	3.0	0.081	Yes	0.054	Yes	Cygnus 2 N
S106	20 25 25.0	+37 12 30.0	10	−1.0	0.103	No	0.034	Yes	GL 2584
CRL 2591	20 27 35.9	+40 01 16.4	28	−22.0	...	...	0.062	No	AGCRL 19
W75N OH	20 36 50.5	+42 27 01.0	3	15.0	0.066	Yes	0.086	Yes	
W75S (1)	20 37 13.3	+42 13 57.0	3	13.0	0.074	Yes	0.054	Yes	
W75S (2A+2B)	20 37 13.8	+42 12 11.0	3	0.0	0.034	Yes	0.069	Yes	
DR 21S	20 37 13.8	+42 08 52.0	3	−6.0	0.091	Yes	0.024	Yes	
W75S (3)	20 37 16.7	+42 15 15.0	3	−4.0	0.057	Yes	0.088	Yes	
PV Cephei	20 45 23.1	+67 46 31.0	29	0.0	0.147	No	0.050	No	
V1057 Cyg	20 57 06.2	+44 03 46.0	30	0.0	...	...	0.064	No	
IRAS 21144+5430	21 14 24.1	+54 30 57.0	31	−88.0	0.110	No	...	...	
S128	21 30 36.6	+55 40 11.0	32	−75.0	0.191	No	...	...	
V645 Cyg	21 38 10.6	+50 00 43.0	14	−44.0	...	...	0.052	No	
NGC 7129 (1)	21 41 52.0	+65 49 40.0	10	−10.0	0.110	Yes	0.030	Yes	GGD 32–35
NGC 7129 (2)	21 41 58.3	+65 53 10.0	10	−10.0	0.061	Yes	0.015	Yes	Lk Hα 234
HHL 73	21 43 14.0	+47 19 15.0	17	−1.0	0.068	Yes	0.075	Yes	
S140	22 17 41.2	+63 03 43.0	2	−9.0	0.080	Yes	0.032	Yes	
S146	22 47 31.0	+59 39 43.0	8	−57.0	0.343	No	0.038	No	
IRC +10523	22 51 40.0	+08 37 54.0	4	...	...	...	...	...	
GGD 37	22 54 19.2	+61 45 44.2	12	0.0	0.154	Yes	0.096	Yes	Cep A
S152	22 55 38.2	+58 33 08.0	2	−52.0	0.199	No	0.019	No	
NGC 7538S	23 11 36.3	+61 10 29.5	3	−55.0	0.110	Yes	0.053	Yes	S158
NGC 7538 IR	23 11 36.5	+61 11 49.5	3	−59.0	0.103	Yes	0.038	Yes[b]	S158
S157	23 13 53.1	+59 45 18.0	3	−46.0	0.089	Yes	0.024	Yes	
IRAS 23151+5912	23 15 08.7	+59 12 25.0	33	−53.4	0.148	No	...	...	

[a] Known interstellar H_2O masers with $\delta > -38°$ in 1986 August.
[b] Detection has been obtained by adding several positions from a five-points map.
[c] Includes G32.80+0.19 (1) and G32.80+0.19 (2).
[d] Includes G32.75+0.08.

References.—(1) Dinger & Dickinson 1980; (2) Genzel & Downes 1979; (3) Genzel & Downes 1977; (4) Blair et al. 1980; (5) Anglada et al. 1989; (6) Rodríguez & Cantó 1983; (7) Comoretto et al. 1990; (8) Henkel et al. 1986; (9) Verdes-Montenegro et al. 1989; (10) Cesarsky et al. 1978; (11) Haschick et al. 1983; (12) Rodríguez et al. 1989; (13) Lada & Wooden 1979; (14) Lada et al. 1981; (15) Batchelor et al. 1980; (16) Blitz & Lada 1979; (17) Gyulbudaghian et al. 1987; (18) Caswell et al. 1983a; (19) Rodríguez et al. 1978; (20) Moran & Rodríguez 1980; (21) Caswell et al. 1983b; (22) Jaffe et al. 1981; (23) Yngvesson et al. 1975; (24) Matthews et al. 1985; (25) Blair et al. 1978; (26) Scalise & Monteiro do Vale 1987; (27) Evans et al. 1979; (28) White & Macdonald 1979; (29) Torrelles et al. 1986; (30) Rodríguez et al. 1987; (31) Gyulbugaghian et al. 1990; (32) Wouterloot et al. 1988; (33) Scalise et al. 1989.

TABLE 2

PARAMETERS OF THE CS AND NH_3 EMISSION

REGION	CS			NH_3		
	T_A^* (K)	V (km s^{-1})	ΔV (km s^{-1})	T_A^* (K)	V (km s^{-1})	ΔV (km s^{-1})
S184	0.33 ± 0.03	−30.80 ± 0.16	3.26 ± 0.38	0.23 ± 0.02	−30.74 ± 0.09	2.72 ± 0.21
W3 (1)	...	...	...	0.09 ± 0.01	−43.22 ± 0.22	2.86 ± 0.51
W3 (2A+2B)	0.22 ± 0.01	−40.34 ± 0.12	4.22 ± 0.30	...	...	
W3 (3)	0.55 ± 0.07	−39.26 ± 0.07	1.15 ± 0.17	0.14 ± 0.01	−38.65 ± 0.08	2.59 ± 0.20
W3 (OH)	0.85 ± 0.02	−46.77 ± 0.04	4.10 ± 0.09	0.15 ± 0.01	−47.59 ± 0.21	5.34 ± 0.52
L1448 N	...	...	...	1.43 ± 0.02	4.37 ± 0.01	1.24 ± 0.02
GL 490	0.50 ± 0.06	−12.95 ± 0.15	2.56 ± 0.37	...	...	...
HH 7–11(B)	1.04 ± 0.03	8.09 ± 0.02	2.00 ± 0.06	0.64 ± 0.03	7.98 ± 0.05	1.90 ± 0.12
AFGL 5142	...	...	...	0.26 ± 0.01	−3.38 ± 0.06	2.86 ± 0.14
Orion KL-A	1.16 ± 0.05	9.03 ± 0.10	4.82 ± 0.24	0.89 ± 0.02	8.23 ± 0.06	5.11 ± 0.18
OMC 2 (2)	0.76 ± 0.04	11.27 ± 0.05	1.67 ± 0.11	0.69 ± 0.03	11.45 ± 0.03	1.23 ± 0.07
OMC 2 (1)	0.59 ± 0.03	11.15 ± 0.04	1.58 ± 0.10	0.64 ± 0.06	11.14 ± 0.07	1.52 ± 0.17
HH 1	0.55 ± 0.05	9.25 ± 0.20	4.62 ± 0.47	0.16 ± 0.02	8.88 ± 0.16	2.45 ± 0.39
AFGL 5157	...	...	...	0.30 ± 0.01	−17.99 ± 0.02	1.50 ± 0.05
GGD 4	0.44 ± 0.05	2.41 ± 0.16	3.05 ± 0.38	0.33 ± 0.01	2.36 ± 0.04	1.69 ± 0.09
S235	0.55 ± 0.08	−16.60 ± 0.14	1.62 ± 0.33	0.15 ± 0.01	−16.83 ± 0.15	3.31 ± 0.35
NGC 2024	1.14 ± 0.04	10.67 ± 0.04	2.72 ± 0.10	0.36 ± 0.01	10.94 ± 0.06	2.85 ± 0.13
HH 19–27	0.66 ± 0.04	10.41 ± 0.04	1.30 ± 0.09	0.33 ± 0.01	10.30 ± 0.03	1.38 ± 0.07
NGC 2071	0.54 ± 0.03	9.58 ± 0.09	2.97 ± 0.22	0.56 ± 0.01	9.38 ± 0.02	1.71 ± 0.05
Mon R2 (1)	0.90 ± 0.04	10.68 ± 0.05	2.58 ± 0.13	0.38 ± 0.02	10.75 ± 0.05	2.13 ± 0.12
Mon R2 (2)	1.02 ± 0.09	10.57 ± 0.22	2.61 ± 0.53	0.29 ± 0.02	10.48 ± 0.08	2.81 ± 0.18
S252A	0.14 ± 0.02	8.33 ± 0.24	4.19 ± 0.57	...	...	...
S252A3	0.77 ± 0.02	8.90 ± 0.04	3.05 ± 0.10	0.27 ± 0.01	8.56 ± 0.06	3.06 ± 0.14
G188.94+0.89	0.68 ± 0.02	3.15 ± 0.04	3.31 ± 0.10	0.20 ± 0.01	3.01 ± 0.10	2.69 ± 0.24
GGD 12–15	0.79 ± 0.03	11.47 ± 0.03	2.16 ± 0.08	0.36 ± 0.02	11.24 ± 0.05	2.22 ± 0.13
S255/257	0.70 ± 0.03	7.52 ± 0.07	3.03 ± 0.17	0.21 ± 0.02	7.47 ± 0.17	3.61 ± 0.41
GGD 16–17	...	...	...	0.22 ± 0.05	12.62 ± 0.28	2.83 ± 0.67
NGC 2264	1.04 ± 0.02	7.63 ± 0.03	4.05 ± 0.08	0.37 ± 0.02	7.88 ± 0.05	2.70 ± 0.13
GL 1074	0.27 ± 0.04	55.10 ± 0.11	1.28 ± 0.25	...	...	...
HHL 50	0.54 ± 0.05	19.80 ± 0.16	3.12 ± 0.38	0.10 ± 0.02	20.25 ± 0.11	1.47 ± 0.27
G354.61+0.47	...	...	...	0.36 ± 0.04	−21.00 ± 0.12	2.49 ± 0.27
G353.41−0.36	...	...	...	0.80 ± 0.08	5.18 ± 0.32	6.69 ± 0.77
G356.64−0.33	1.05 ± 0.00	...	...	0.51 ± 0.08	−17.62 ± 0.29	3.59 ± 0.70
G359.97−0.46	0.95 ± 0.10	18.58 ± 0.13	2.59 ± 0.31	0.36 ± 0.07	18.49 ± 0.17	2.17 ± 0.41
RCW 142	2.01 ± 0.06	17.06 ± 0.08	5.68 ± 0.18	0.60 ± 0.05	16.13 ± 0.17	4.30 ± 0.41
W28A2	1.93 ± 0.06	9.37 ± 0.06	4.24 ± 0.15	0.42 ± 0.06	9.42 ± 0.23	3.50 ± 0.54
W31 (2)	1.75 ± 0.04	−3.04 ± 0.06	5.37 ± 0.15	0.37 ± 0.06	−2.73 ± 0.15	1.81 ± 0.35
G12.76+0.33	0.45 ± 0.05	18.78 ± 0.20	1.57 ± 0.49	0.19 ± 0.04	16.54 ± 0.24	2.50 ± 0.56
G12.21−0.10	...	...	...	0.35 ± 0.03	27.52 ± 0.14	3.16 ± 0.34
G12.21−0.12	...	...	...	0.29 ± 0.03	28.09 ± 0.24	3.31 ± 0.56
W33B	...	...	...	0.36 ± 0.03	54.50 ± 0.25	5.34 ± 0.63
G13.19+0.04	...	...	...	0.37 ± 0.06	50.78 ± 0.15	1.82 ± 0.36
W33A	0.66 ± 0.05	36.72 ± 0.19	5.22 ± 0.46	...	...	...
G14.45−0.11	...	...	...	0.45 ± 0.04	40.01 ± 0.18	4.06 ± 0.42
G13.66−0.60	0.37 ± 0.06	47.95 ± 0.32	1.41 ± 0.80	0.29 ± 0.03	47.67 ± 0.12	2.04 ± 0.28
G14.23−0.51	0.97 ± 0.04	19.81 ± 0.08	3.68 ± 0.19	0.41 ± 0.04	19.68 ± 0.12	2.38 ± 0.29
W37	0.18 ± 0.02	23.26 ± 0.35	6.23 ± 0.85	...	...	...
G14.33−0.64	0.84 ± 0.04	21.99 ± 0.10	4.17 ± 0.24	0.58 ± 0.04	23.17 ± 0.18	4.96 ± 0.44
G14.63−0.58	0.63 ± 0.05	18.92 ± 0.13	3.33 ± 0.30	0.44 ± 0.04	18.49 ± 0.11	2.90 ± 0.27
M17 (1)	...	...	...	0.40 ± 0.03	18.96 ± 0.12	3.87 ± 0.28
M17 (2+3)	1.58 ± 0.07	19.82 ± 0.10	4.33 ± 0.24	0.34 ± 0.02	19.52 ± 0.10	4.02 ± 0.23
G16.58−0.05	...	...	...	0.19 ± 0.01	59.68 ± 0.11	2.95 ± 0.26
G16.61−0.05	...	...	...	0.10 ± 0.01	59.53 ± 0.20	3.40 ± 0.40
G19.61−0.13	0.26 ± 0.03	59.67 ± 0.19	2.95 ± 0.46	...	...	...
G19.60−0.23	...	...	...	0.29 ± 0.06	20.61 ± 0.10	1.02 ± 0.23
G20.78−0.05	...	...	...	0.33 ± 0.07	61.41 ± 0.22	1.30 ± 0.51
GGD 29	0.63 ± 0.03	8.25 ± 0.05	2.12 ± 0.13	0.61 ± 0.04	8.15 ± 0.05	1.62 ± 0.12
G22.36+0.07	...	...	...	0.09 ± 0.01	84.29 ± 0.31	3.94 ± 0.73
G21.37−0.61	...	...	...	0.11 ± 0.02	55.32 ± 0.16	1.33 ± 0.38
G23.95+0.15	0.55 ± 0.03	79.97 ± 0.08	3.25 ± 0.19	0.12 ± 0.01	80.08 ± 0.27	4.71 ± 0.65
G23.01−0.41	0.32 ± 0.02	76.50 ± 0.13	5.61 ± 0.33	0.37 ± 0.03	77.02 ± 0.14	3.60 ± 0.34
G24.49−0.04	0.39 ± 0.02	110.35 ± 0.10	4.14 ± 0.25	0.16 ± 0.02	110.05 ± 0.21	3.80 ± 0.49
G24.79+0.08	0.59 ± 0.03	110.32 ± 0.12	4.78 ± 0.29	0.39 ± 0.02	109.55 ± 0.09	3.73 ± 0.21
G28.86+0.07	0.51 ± 0.03	103.28 ± 0.10	3.35 ± 0.25	...	...	...
W43S	...	...	...	0.28 ± 0.05	97.55 ± 0.32	3.16 ± 0.75
G31.41+0.31	0.53 ± 0.04	97.11 ± 0.13	3.38 ± 0.30	0.24 ± 0.02	95.99 ± 0.14	3.34 ± 0.34
W43 Main (2)	...	...	...	0.28 ± 0.03	95.20 ± 0.35	7.99 ± 0.86
W43 Main (3)	0.45 ± 0.01	97.03 ± 0.13	9.48 ± 0.33	0.40 ± 0.02	96.99 ± 0.30	8.70 ± 0.80
W43 Main (4)	...	...	...	0.13 ± 0.03	111.29 ± 0.11	0.93 ± 0.27
G31.29+0.07	0.32 ± 0.02	108.28 ± 0.19	5.97 ± 0.47	0.26 ± 0.03	107.79 ± 0.25	4.65 ± 0.51
G31.25−0.11	...	...	...	0.09 ± 0.01	−9.85 ± 0.27	3.45 ± 0.63

TABLE 2—*Continued*

Region	CS			NH_3		
	T_A^* (K)	V (km s^{-1})	ΔV (km s^{-1})	T_A^* (K)	V (km s^{-1})	ΔV (km s^{-1})
G32.15+0.13	0.23 ± 0.03	94.00 ± 0.19	3.50 ± 0.45	0.31 ± 0.03	94.12 ± 0.20	4.11 ± 0.48
G32.04+0.06	0.48 ± 0.03	95.76 ± 0.20	3.62 ± 0.50	0.36 ± 0.04	95.08 ± 0.18	3.48 ± 0.43
G32.10−0.08	...	...	...	0.18 ± 0.03	47.94 ± 0.28	3.13 ± 0.67
G32.74−0.08	...	...	...	0.14 ± 0.02	38.24 ± 0.39	5.10 ± 0.92
G33.91+0.11	0.42 ± 0.03	106.34 ± 0.21	5.53 ± 0.51	0.43 ± 0.04	107.61 ± 0.12	2.70 ± 0.28
W44	1.02 ± 0.05	57.52 ± 0.09	3.98 ± 0.22	0.58 ± 0.04	58.08 ± 0.13	4.29 ± 0.32
G35.03+0.3	0.42 ± 0.05	52.68 ± 0.14	2.58 ± 0.34	0.25 ± 0.05	52.05 ± 0.12	1.27 ± 0.28
S76W	...	...	...	0.20 ± 0.03	32.53 ± 0.17	1.98 ± 0.41
S76E	0.65 ± 0.03	33.08 ± 0.07	3.18 ± 0.16	0.32 ± 0.02	32.72 ± 0.09	3.07 ± 0.22
G35.20−0.74	0.87 ± 0.06	34.40 ± 0.16	4.71 ± 0.39	0.54 ± 0.06	33.54 ± 0.14	2.66 ± 0.34
W48	0.53 ± 0.02	43.08 ± 0.07	4.27 ± 0.17	0.48 ± 0.09	42.54 ± 0.12	1.28 ± 0.29
G40.62−0.14	0.36 ± 0.02	33.13 ± 0.14	4.58 ± 0.33	0.23 ± 0.05	34.40 ± 0.29	3.38 ± 0.69
G45.49+0.13	0.32 ± 0.02	60.83 ± 0.17	5.74 ± 0.41	...	...	...
G45.44+0.07	0.20 ± 0.02	58.00 ± 0.23	5.91 ± 0.56	...	...	...
W51 Main/S	1.76 ± 0.01	56.88 ± 0.04	10.41 ± 0.10	0.58 ± 0.01	54.80 ± 0.20	8.30 ± 0.40
S87	0.50 ± 0.02	22.91 ± 0.10	4.35 ± 0.25	0.38 ± 0.06	23.64 ± 0.16	2.28 ± 0.39
K3-50	...	...	...	0.37 ± 0.07	−2.01 ± 0.19	1.94 ± 0.45
ON 3	0.35 ± 0.02	−22.60 ± 0.11	4.58 ± 0.26	...	...	...
ON 1	0.56 ± 0.02	11.27 ± 0.06	4.18 ± 0.16	0.56 ± 0.03	11.00 ± 0.07	2.67 ± 0.18
ON 2S	0.58 ± 0.02	−.97 ± 0.08	5.14 ± 0.20	0.36 ± 0.02	−1.45 ± 0.11	3.53 ± 0.27
ON 2N	0.26 ± 0.03	−.62 ± 0.16	3.18 ± 0.38	0.23 ± 0.05	−.14 ± 0.15	1.49 ± 0.35
S106	...	...	...	0.24 ± 0.03	−.98 ± 0.07	1.26 ± 0.16
W75N OH	0.91 ± 0.02	9.49 ± 0.04	3.55 ± 0.11	0.32 ± 0.04	9.47 ± 0.22	3.64 ± 0.52
W75S (1)	1.27 ± 0.02	−3.37 ± 0.03	3.20 ± 0.07	1.11 ± 0.07	−3.58 ± 0.07	2.31 ± 0.16
W75S (2A+2B)	1.61 ± 0.02	−3.04 ± 0.02	4.13 ± 0.05	0.96 ± 0.03	−3.50 ± 0.06	3.31 ± 0.14
DR 21S	1.24 ± 0.03	−2.44 ± 0.03	3.11 ± 0.08	0.22 ± 0.01	−2.48 ± 0.10	3.60 ± 0.24
W75S (3)	1.02 ± 0.02	−3.71 ± 0.03	3.39 ± 0.08	0.69 ± 0.06	−4.12 ± 0.08	1.79 ± 0.18
NGC 7129 (1)	0.43 ± 0.05	−10.00 ± 0.10	1.66 ± 0.24	0.24 ± 0.02	−9.89 ± 0.07	1.54 ± 0.16
NGC 7129 (2)	0.20 ± 0.02	−9.90 ± 0.13	2.51 ± 0.31	0.14 ± 0.01	−10.34 ± 0.06	1.27 ± 0.13
HHL 73	0.33 ± 0.04	3.99 ± 0.07	1.34 ± 0.17	0.34 ± 0.06	3.56 ± 0.10	1.21 ± 0.23
S140	1.36 ± 0.05	−7.05 ± 0.05	2.72 ± 0.11	0.32 ± 0.02	−7.22 ± 0.07	2.28 ± 0.18
GGD 37	0.88 ± 0.05	−10.68 ± 0.10	3.79 ± 0.24	0.46 ± 0.05	−10.24 ± 0.13	2.34 ± 0.32
NGC 7538S	1.22 ± 0.02	−56.52 ± 0.03	4.91 ± 0.08	0.63 ± 0.02	−56.31 ± 0.08	4.92 ± 0.20
NGC 7538 IR	0.65 ± 0.03	−56.48 ± 0.09	4.15 ± 0.21	0.47 ± 0.02	−56.57 ± 0.08	3.75 ± 0.22
S157	0.32 ± 0.02	−43.47 ± 0.13	3.57 ± 0.32	0.06 ± 0.01	−43.37 ± 0.38	4.50 ± 0.90

(58%; 104 of 179 H_2O maser sources). In a much smaller sample, Zinchenko et al. (1995) detected CS ($J = 2 \rightarrow 1$) in 27 of 29 H_2O masers.

In our survey, the detection rates of the two molecules for the regions observed both in CS and in NH_3 were very similar (Table 4). Of the 99 regions observed in CS and NH_3, 75 were detected in CS, while 77 were detected in NH_3, 66 being detected in both molecular transitions. These results seem to indicate that the CS and NH_3 molecules are excited under similar physical conditions.

4. DISCUSSION

4.1. *Comparison of the* CS *and* NH_3 *Emissions*

In a previous work, Pastor et al. (1991) compared in detail maps of the CS ($J = 1 \rightarrow 0$) and NH_3 (J, K) = (1, 1) emissions in several star-forming regions. In the present work we observed CS and NH_3 spectra toward a large number of H_2O maser positions. This allowed us to make a statistically more significant comparison between the CS and NH_3 emissions, but restricted to the spectral parameters and to a single position per source, thus lacking the information about the extension of the emission.

TABLE 3

Summary of the Sources Observed in CS or NH_3

	CS	NH_3
Observed sources	107	164
Detected sources (SNR > 5)	75	82
Detected sources (3 < SNR < 5)	2	13
Nondetected sources (SNR < 3)	30	69

4.1.1. *Line Intensities*

In Figure 1 we show the plot of the CS line intensities (as measured by the corrected antenna temperature) versus NH_3 line intensities for the sources that were detected in both molecules. The CS line intensities are, in general, greater than that of NH_3. The distribution of the ratio $T_A^*(\mathrm{CS})/T_A^*(\mathrm{NH_3})$ has an average of 2.3, with a lower limit of 0.7 and an upper limit of 5.7.

The difference in line intensity between the two molecules could be attributed to differences in the excitation temperature or optical depth of the two transitions. However, the different coupling factor of the sources with the antenna beam at the two frequencies can also explain the difference observed in the line intensities.

As is shown in the Appendix, for the Haystack antenna and a uniform circular source of the same size at the two frequencies, the value of the ratio $T_A^*(\mathrm{CS})/T_A^*(\mathrm{NH_3})$ ranges from 0.28 for extended sources (because of the difference in beam efficiency at the two frequencies) to 1.2 for unresolved sources (because of the difference in beam size and aperture efficiency). Since the size of the sources in CS is in general larger than in NH_3, this ratio can be higher. For instance, Pastor et al. (1991) found that the median ratio of sizes of sources in CS ($J = 1 \rightarrow 0$) and NH_3 (J, K) = (1, 1) is 2.3. For

TABLE 4

SUMMARY OF THE SOURCES OBSERVED BOTH IN CS AND NH_3

	Detected in CS (SNR > 5)	Detected in CS (3 < SNR < 5)	Nondetected in CS (SNR < 3)
Detected in NH_3 (SNR > 5)	61	1	9
Detected in NH_3 (3 < SNR < 5).....	4	0	2
Nondetected in NH_3 (SNR < 3)	8	1	13

this value of the source size ratio, the ratio $T_A^*(CS)/T_A^*(NH_3)$ can be as high as 6.4 for unresolved sources (see Fig. 16 in the Appendix).

Thus, the differences in the coupling factors of the sources with the antenna beam can easily account for the observed range of the ratio of the line intensities.

4.1.2. *Line Widths*

In our sample, the observed line widths typically lie between 2 and 5 km s^{-1} for CS ($\sim$72% of the sources) and between 1 and 4 km s^{-1} for NH_3 ($\sim$75% of the sources) (Table 2). Churchwell et al. (1990), from a study of the NH_3 and H_2O emissions in a sample of ultracompact H II regions, obtain a similar result (71% of the sources with NH_3 line widths between 1.5 and 4 km s^{-1}).

In Figures 2 and 3 we show the distribution of the CS and NH_3 line widths, corrected for the spectral channel width. The average of ΔV(CS) is 3.7 km s^{-1} while the average of $\Delta V(NH_3)$ is 3.0 km s^{-1}. Churchwell et al. (1990) find a similar average, $\Delta V(NH_3) = 3.1$ km s^{-1}, for a sample in which most sources are associated with H_2O masers. These NH_3 line widths are significantly larger than those found in other regions not associated with H_2O maser emission. For instance, Benson & Myers (1989), in a study on dense condensations in dark clouds, find $\Delta V(NH_3) = 0.45$ km s^{-1} for condensations associated with a star, and $\Delta V(NH_3) = 0.27$ km s^{-1} for condensations without a star. These figures correspond to the intrinsic widths of the hyperfine components, and hence they cannot be directly compared with ours. However, if one takes into account the hyperfine broadening as a function of opacity (Ho 1977), these intrinsic line widths would correspond, even for high opacities, to observed line widths less than 1.5 km s^{-1}, which is significantly smaller than the line widths obtained by us and by Churchwell et al. (1990). Zinchenko et al. (1995) also obtained large CS ($J = 2 \rightarrow 1$) line widths in a sample of H_2O masers. These results, therefore, seem to indicate that the H_2O maser emission is associated with a notable perturbation of the dense molecular gas, which is reflected in a significant broadening of the lines.

The distribution of the CS line widths is shifted toward larger line widths than that of NH_3 (see Figs. 2 and 3). These significant differences between the widths of the two lines, the CS lines being generally broader than the NH_3 ones, have been previously found in other regions (see, e.g., Pastor et al. 1991 and references therein). Both distributions have very similar standard deviations ($\sim$1.6 km s^{-1}), though they differ in shape. For the case of NH_3, there is a large difference in the number of sources between the first and the second bins (corresponding, respectively, to line widths less and greater than 0.75 km s^{-1}). This is probably a consequence of not having corrected the NH_3 line widths for the effects of opacity and overlapping of hyperfine components.

In Figure 4 we compare the CS and the NH_3 line widths, corrected for the spectral channel width, for sources clearly detected (SNR > 5) in both molecules (a total of 61 sources). As the errors in the CS and the NH_3 line widths are similar

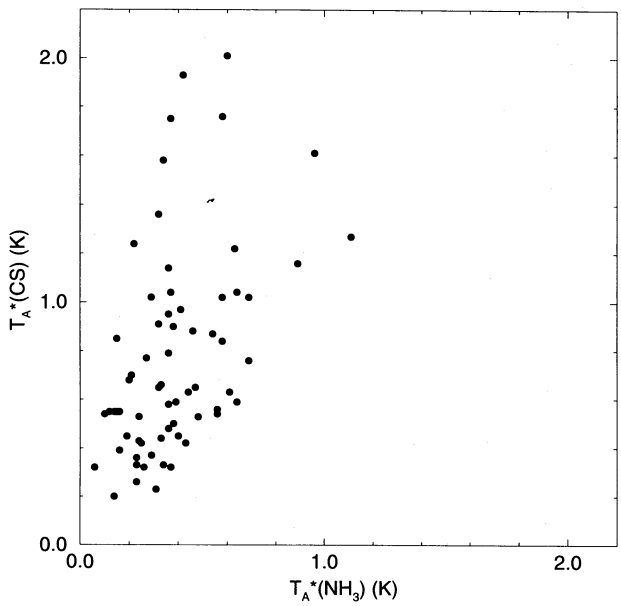

FIG. 1.—Plot of the CS line intensities vs. the NH_3 line intensities for the sources that were detected in both molecules.

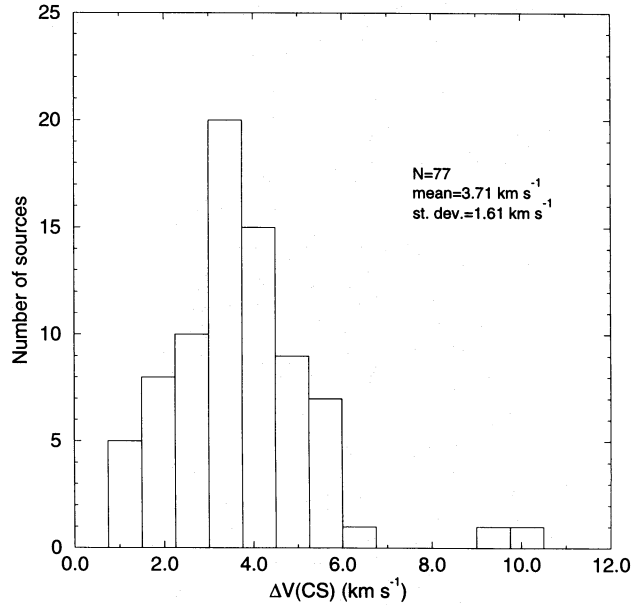

FIG. 2.—Distribution of the CS line widths for the detected sources. We also give in the figure the statistical parameters of the distribution.

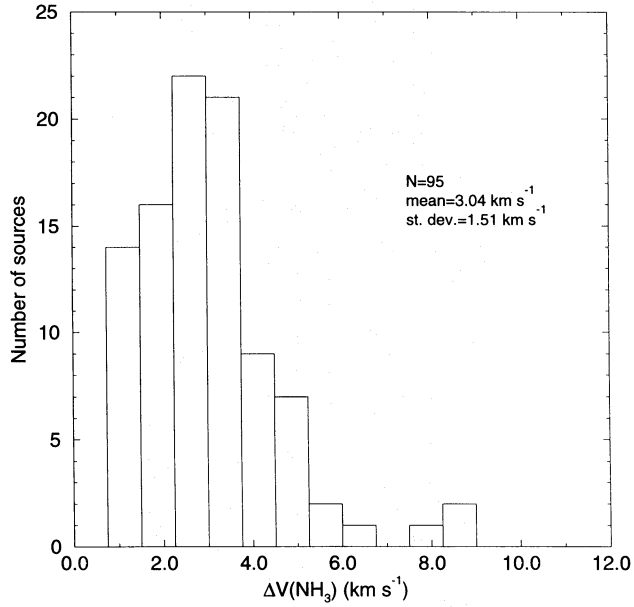

FIG. 3.—Distribution of the NH_3 line widths for the detected sources. We also give in the figure the statistical parameters of the distribution.

(see Table 2), we performed a linear fit to the data considering the same error in both axes. The fit gives

$$\Delta V(\mathrm{CS}) = 1.1\Delta V(\mathrm{NH_3}) + 0.3 \text{ km s}^{-1}, \quad (1)$$

with a correlation coefficient $r = 0.8$. This result suggests that the difference between the CS and NH_3 line widths is better described as an additive term than as a multiplicative factor. The fit obtained from our sample is very similar to that obtained by Pastor et al. (1991) from a detailed study of six star-forming regions. Thus, we confirm with a large sample of sources the relationship obtained by Pastor et al. (1991), and we extend its validity up to larger line widths (~ 10 km s^{-1} vs. ~ 2 km s^{-1}).

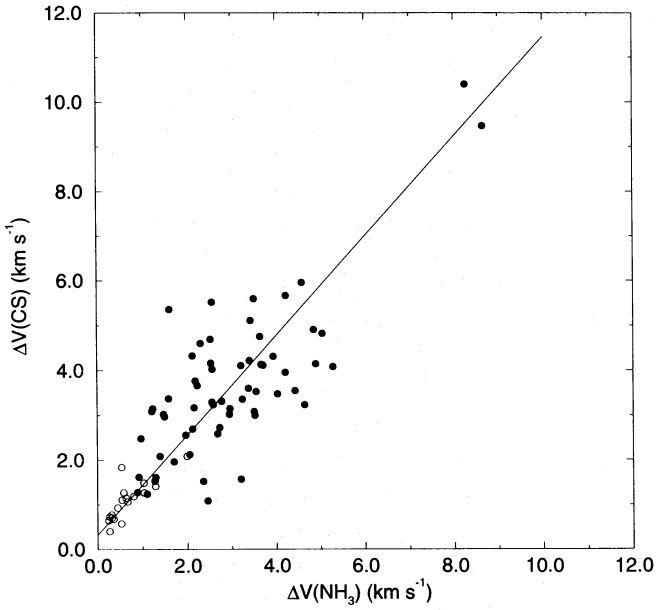

FIG. 4.—Plot of the CS line widths vs. the NH_3 line widths, for the sources that were detected with SNR > 5 in both molecules (*filled circles*). The CS and NH_3 line widths have been corrected for the spectral channel width. The straight line is the best linear fit (considering the same error in both axes) to the data. The data from Pastor et al. (1991) are also shown (*open circles*).

The fact that the CS lines are wider than those of the NH_3 may indicate that CS traces regions dynamically more active. This could happen, for instance, if the dynamics of the cloud affects the chemistry of these molecules. Alternatively, the difference in line widths could be attributed to differences in the size in the region traced by each molecule. It is well known (e.g., Larson 1981) that the line width correlates with the size of the cloud, although the physical basis of this correlation, which is related with the role of the internal motions in the cloud support, is still not well established. For the nonthermal component of the line width, the line width–size relation goes as $\Delta V_{\mathrm{NT}} \propto R^q$, with the index $q \simeq 0.5$ for low-mass cores, and $q \simeq 0.2$ for high-mass cores (e.g., Caselli & Myers 1995). If the fact that CS lines are found to be broader than those of NH_3 is interpreted in terms of this relationship, this would imply that regions traced by CS should be larger than those traced by NH_3. Although from our data we do not obtain direct information about the cloud size, it is a general result that, for regions mapped in both molecules, the CS emission is found to be more extended than that of the NH_3 (see, e.g., Zhou et al. 1989; Pastor et al. 1991), in agreement with this interpretation. If the difference between CS and NH_3 line widths is an additive term as our results suggest, this would imply that the ratio between CS and NH_3 sizes, $R(\mathrm{CS})/R(\mathrm{NH_3})$, should be higher for smaller sources. A difference in line width of 0.3 km s^{-1} represents, for the line width–size relation given by Caselli & Myers (1995) for high-mass cores (which seems more adequate for our sources), that the ratio $R(\mathrm{CS})/R(\mathrm{NH_3}) \simeq 3$ for sources of the order of 0.1 pc and $R(\mathrm{CS})/R(\mathrm{NH_3}) \simeq 2$ for sources of the order of 1 pc. These values for the size ratio are consistent with the (limited) currently available comparative studies (see, e.g., Pastor et al. 1991; Morata et al. 1996) of regions mapped in CS and NH_3.

4.1.3. *Velocities*

In Figure 5, the central velocities of the CS spectra have been plotted versus those of the NH_3 spectra. The result of the best linear fit to the data (considering the same error in both axes) is

$$V(\mathrm{CS}) = 1.00V(\mathrm{NH_3}) + 0.12 \text{ km s}^{-1}, \quad (2)$$

with a correlation coefficient $r = 1.0$. This relation indicates that both molecules are roughly tracing the same region. Given the large number of sources observed, we are able to measure small discrepancies. Particularly, it can be noted that this straight line with unity slope does not pass through the origin. Figure 6 shows that the distribution of the difference $V(\mathrm{CS}) - V(\mathrm{NH_3})$ is not centered on zero (mean = 0.15 ± 0.07 km s^{-1}). Although this is only a 2 σ result, it is rather significant since the probability of obtaining a value outside the 2 σ interval is only 5%. This result and the symmetry of the distribution about its mean value suggest that there is a real systematic shift of the CS line velocities relative to the NH_3 ones.

The CS observations were made using a nominal value for the frequency of the $J = 1 \rightarrow 0$ transition of 48.990968 GHz, while 48.990964 GHz is the value recommended at present (Lovas 1986). Due to this small difference, the measured velocities of the CS lines must be corrected by -0.024 km s^{-1}. After this correction, the mean value of the difference in velocity is $V(\mathrm{CS}) - V(\mathrm{NH_3}) = 0.12 \pm 0.07$ km s^{-1}. The estimated uncertainty of the theoretically predicted fre-

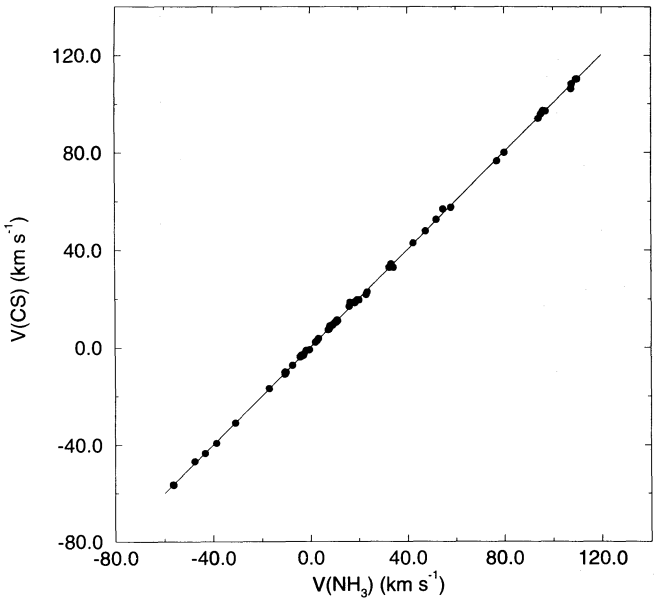

FIG. 5.—Plot of the central velocity of the CS lines vs. the central velocity of the NH_3 lines. The straight line is the best linear fit (considering the same error in both axes) to the data.

quencies of the two transitions is 4.5 kHz for the CS and 0.05 kHz for the NH_3 (1 σ; Lovas 1986), which corresponds to an uncertainty in the difference in velocity of 0.03 km s^{-1}. Therefore, it is plausible that at least part of the observed difference in the CS and NH_3 velocities is real and not a consequence of the poor knowledge of the frequencies. This difference could have an instrumental origin. As was pointed out in § 3, a correction of $\sim$0.2 km s^{-1} was applied to the line velocities in order to correct for the errors introduced by the Haystack Observatory autocorrelator (Ball & Haschick 1988; Ball 1989). Since before applying these corrections the difference in velocity was of the same order but opposite in sign, this could indicate that the correction has been overestimated. Benson & Myers (1989) found a difference of 0.07 km s^{-1} between the velocities of $C^{18}O$ and those of NH_3, for a sample of 18 sources. Alternatively, the observed velocity shift between CS and NH_3 lines might have a physical origin as a consequence of opacity effects in clouds dominated by systematic (expanding/contracting) motions. As CS tends to trace larger regions than NH_3 (Pastor et al. 1991; see also §§ 4.1.1 and 4.1.2) and because of opacity effects, the CS emission will tend to present a larger contribution from the outer part of the cloud nearest to the observer, while the NH_3 traces preferentially the core of the cloud. As we find that CS is slightly redshifted with respect to NH_3, this could indicate a trend to the presence of infall motions in the outer parts of the cloud. However, we note that this is only a minor effect in our data, from which no strong physical constraints can be derived.

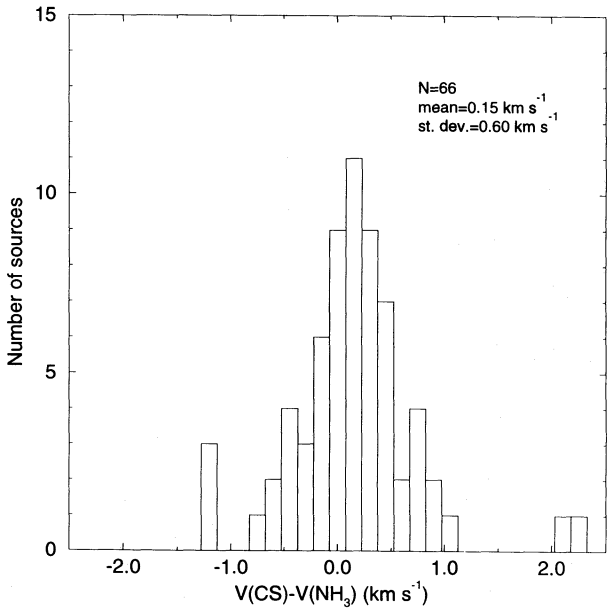

FIG. 6.—Distribution of the difference in the central velocity between the CS and the NH_3 lines for the sources that were detected in both molecules. We also give in the figure the statistical parameters of the distribution.

The distribution of the difference in velocity between CS and NH_3 (Fig. 6) has a standard deviation of 0.6 km s^{-1}. This is a relatively high value when compared with the results obtained in other studies, such as Pastor et al. (1991), where they find that these two velocities agree within $\sim$0.1 km s^{-1}. This fact further suggests that the CS and NH_3 emissions, although roughly originating in the same region, are not tracing exactly the same beam averaged column density of gas. This can be due to differences in the size of the emitting region or to differences in the opacity and excitation between these two molecules. Given the large number of sources in our sample, one expects to find some regions with large velocity inhomogeneities, i.e., large velocity gradients or turbulence, and thus, larger differences between the CS and the NH_3 velocities. The existence of large velocity inhomogeneities is also supported by the large line widths (up to 10 km s^{-1}) found in some regions of our sample, whereas Pastor et al. (1991) found maximum line widths of $\sim$3 km s^{-1}.

4.2. *The H_2O Maser Sample*

In this section we study the parameters of the H_2O maser emission in order to analyze how it is related to the CS and NH_3 emissions. Hereafter, unless indicated otherwise, we will consider only the H_2O masers toward whose positions CS or NH_3 emission has been detected. In Table 5 we give the parameters that characterize these H_2O masers. The characterization of the H_2O maser emission is difficult because of its high temporal variability. Since we compiled this table in 1991, only references prior to this date were used. In making Table 5, in general, we took into account different observations for each source, although the list of references used for each source (given in the table) was not intended to be exhaustive. We estimated from the published plots of the spectra those parameters not explicitly given in the references.

In Table 5 we give the minimum and maximum of the velocity range over which the H_2O maser emission extends, V_{min} and V_{max}. These are the minimum and maximum velocities at which some emission component appears in any of the spectra used for each source.

For each H_2O maser spectrum we determined the velocity of the maximum of the emission, the mean velocity of the detected components, and the intensity-weighted mean velocity. In Table 5 we give, for each source, the velocity of the absolute maximum of all the spectra, $V_m(H_2O)$; the average, for all the spectra, of the mean velocities, $V_a(H_2O)$; and the average, for all the spectra, of the weighted mean

TABLE 5

PARAMETERS OF H_2O MASER SOURCES DETECTED IN CS OR NH_3

REGION	$V(H_2O)$ (km s^{-1}) V_{min}[a]	V_{max}[b]	V_m[c]	V_a[d]	V_c[e]	REFERENCES	V_0[f] (km s^{-1})	D (kpc)	REFERENCES	$L(H_2O)$[g] ($L_\odot$)
S184	−43.0	−13.9	−31.3	−31.6	−31.4	1, 2, 3, 4	−30.8	2.2	5	1.0×10^{-5}
W3 (1)	−52.7	−33.8	−34.3	−46.0	−44.3	4, 6	−43.2	2.4	7	7.3×10^{-5}
W3 (2A+2B)	−52.0	−33.4	−40.5	−40.1	−39.5	4, 6	−40.3	2.4	7	2.0×10^{-4}
W3 (3)	−68.7	−30.7	−38.8	−46.2	−41.7	4, 6, 8	−39.0	2.4	7	1.5×10^{-5}
W3 (OH)	−62.0	−31.2	−48.8	−48.6	−48.2	4, 6	−47.2	2.4	7	4.2×10^{-3}
L1448N	2.6	3.3	3.3	3.0	3.3	4, 9	4.4	0.4	10	1.2×10^{-6}
GL 490	−13.0	−13.0	−13.0	−13.0	−13.0	11, 12	−13.0	0.9	13	1.3×10^{-7}
HH 7–11(B)	−15.2	11.0	4.8	6.3	6.7	4, 12, 14	8.0	0.5	15	3.5×10^{-7}
AFGL 5142	−6.8	4.4	−4.8	−2.6	−1.4	16	−3.4	1.8	17	1.6×10^{-5}
Orion KL-A	−50.0	69.0	7.5	12.5	9.2	4, 6, 18	8.6	0.5	18	9.5×10^{-4}
OMC 2 (2)	7.0	13.0	7.4	10.6	10.6	4, 8, 11	11.4	0.5	18	4.0×10^{-7}
OMC 2 (1)	4.3	19.1	7.5	12.0	7.8	1, 4, 11, 19	11.1	0.5	18	6.4×10^{-7}
HH 1	2.0	11.1	11.1	5.5	5.5	20, 21	9.1	0.5	22	1.6×10^{-6}
AFGL 5157	−31.9	−3.5	−23.3	−18.4	−18.7	16	−18.0	1.8	17	7.3×10^{-6}
GGD 4	−18.8	11.2	4.0	−3.5	2.0	23	2.4	1.7	23	5.0×10^{-7}
S235	−71.4	2.0	−21.0	−35.5	−36.4	4, 6, 11, 24	−16.7	1.6	5	1.2×10^{-3}
NGC 2024	9.9	27.1	13.1	11.1	11.8	4, 6, 25	10.8	0.5	15	1.4×10^{-6}
HH 19–27	23.4	25.0	23.4	24.6	24.6	20	10.4	0.5	15	2.0×10^{-8}
NGC 2071	−8.0	19.9	15.9	6.7	7.5	4, 25, 26, 27, 28	9.5	0.5	15	5.6×10^{-6}
Mon R2 (1)	10.3	11.9	11.9	11.6	11.7	4, 6, 19, 29	10.7	1.0	30	7.1×10^{-7}
Mon R2 (2)	11.7	11.8	11.7	11.7	11.7	4, 6	10.5	1.0	30	2.0×10^{-6}
S252A	8.0	10.7	9.2	11.1	9.3	31	8.3	2.0	31	...
S252A3	7.0	25.0	7.0	10.9	8.9	1, 4, 31, 32	8.7	2.0	31	1.6×10^{-5}
G188.94+0.89	−5.0	8.5	8.3	2.3	1.3	4, 33	3.1	0.7	34	6.1×10^{-7}
GGD 12–15	−18.5	−6.6	−13.4	−12.6	−12.7	11, 23, 35	11.4	1.0	36	2.0×10^{-6}
S255/257	−0.2	27.5	8.7	11.6	9.7	4, 6, 12, 21, 24, 37	7.5	2.5	38	1.1×10^{-4}
GGD 16–17	7.0	7.0	7.0	7.0	7.0	23	12.6	1.0	36	1.0×10^{-7}
NGC 2264	0.0	18.0	18.0	5.6	7.7	6, 25	7.8	0.8	39	8.0×10^{-7}
GL 1074	40.9	54.9	42.8	47.7	45.5	40, 41	55.1	5.5	34	5.6×10^{-5}
HHL 50	6.5	24.0	24.0	15.3	15.3	4, 42	20.0	1.6	34	7.0×10^{-7}
G354.61+0.47	−11.0	8.5	−11.0	−9.8	−9.9	43	−21.0	...		...
G353.41−0.36	−20.0	−14.2	−20.0	−17.0	−17.3	35	5.2	...		...
G356.64−0.33	−10.0	−10.0	−10.0	−10.0	−10.0	35	−17.6	...		...
G359.97−0.46	19.5	21.0	21.0	21.0	21.0	4, 43	18.5	...		...
RCW 142	−5.0	81.8	17.0	37.5	37.1	4, 6	16.6	...		...
W28A2	7.0	77.0	8.8	18.0	17.2	6, 44, 45	9.4	2.6	46	2.5×10^{-5}
W31 (2)	−15.4	3.9	−1.9	−3.5	−1.5	4, 6, 47	−2.9	6.0	48	1.0×10^{-3}
G12.76+0.33	22.0	22.0	22.0	22.0	22.0	49	17.7	2.3	50	2.0×10^{-6}
G12.21−0.10	−20.1	33.9	−5.6	7.9	10.0	4, 6, 49	27.5	13.4	50	3.0×10^{-2}
G12.21−0.12	−0.1	29.3	26.7	20.3	21.7	4, 6	28.1	13.4	50	1.2×10^{-3}
W33B	54.8	61.5	58.5	58.4	58.7	4, 6, 49	54.5	3.8	50	6.0×10^{-4}
G13.19+0.04	−21.0	1.7	−1.7	−11.3	−11.4	6, 49	50.8	4.7	50	3.6×10^{-5}
W33A	39.0	39.0	39.0	39.0	39.0	6, 49	36.7	3.7	50	2.0×10^{-5}
G14.45−0.11	37.0	61.0	37.0	43.0	38.3	4, 49	40.0	3.8	50	1.3×10^{-5}
G13.66−0.60	41.9	70.3	51.2	50.6	49.2	4, 49	47.8	4.4	50	2.0×10^{-4}
G14.23−0.51	11.4	44.3	25.0	29.2	30.9	4, 49	19.7	2.3	50	4.0×10^{-5}
W37	17.5	17.5	17.5	17.5	17.5	51	23.3	...		...
G14.33−0.64	−8.5	24.9	22.8	16.2	20.8	49	22.6	2.3	50	3.0×10^{-5}
G14.63−0.58	26.4	26.9	26.4	26.4	26.4	49	18.7	2.3	50	4.0×10^{-6}
M17 (1)	−9.1	27.5	13.5	2.9	3.8	4, 6, 49	19.0	2.3	50	4.0×10^{-5}
M17 (2+3)	−37.2	28.8	20.8	9.0	9.0	4, 6,49	19.7	2.3	50	4.0×10^{-5}
G16.58−0.05	57.0	69.5	60.3	61.3	61.1	4, 52	59.7	5.4	53	8.0×10^{-5}
G16.61−0.05	46.0	50.5	46.0	48.3	47.8	52	59.5	5.4	53	8.0×10^{-6}
G19.61−0.13	50.0	55.4	50.0	52.6	52.6	1, 54	59.7	4.5	46	5.1×10^{-5}
G19.60−0.23	16.3	56.1	27.3	39.4	37.3	4, 6	20.6	2.1	34	8.3×10^{-5}
G20.78−0.05	56.4	60.0	60.0	58.2	59.3	54	61.4	11.6	34	1.9×10^{-5}
GGD 29	8.0	40.0	40.0	23.7	24.3	20, 23	8.2	0.4	15	2.0×10^{-7}
G22.36+0.07	88.4	89.9	89.9	89.1	89.5	54	84.3	12.2	53	1.4×10^{-4}
G21.37−0.61	53.0	53.0	53.0	53.0	53.0	1	55.3	4.6	53	8.0×10^{-6}
G23.95+0.15	82.0	82.0	82.0	82.0	82.0	6	80.0	5.8	53	4.6×10^{-5}
G23.01−0.41	73.3	82.3	80.0	77.5	78.4	4, 52	76.8	12.8	53	7.5×10^{-4}
G24.49−0.04	116.0	116.0	116.0	116.0	116.0	1	110.2	8.5	1	6.0×10^{-5}
G24.79+0.08	44.3	119.6	110.5	99.7	99.8	1, 4, 6	109.9	8.5	1	5.0×10^{-4}
G28.86+0.07	91.5	106.8	106.5	92.8	96.4	1, 4	103.3	8.5	1	3.0×10^{-4}
W43S	96.0	102.3	96.7	98.1	98.1	4, 6	97.5	7.4	34	2.3×10^{-4}
G31.41+0.31	94.9	104.3	100.7	99.3	99.6	4, 6	96.5	7.2	34	3.1×10^{-4}
W43 Main (2)	42.5	53.6	48.0	48.5	48.5	4, 6	95.2	7.3	34	6.1×10^{-5}
W43 Main (3)	55.7	124.0	99.5	99.4	101.4	4, 6, 54	97.0	7.3	34	2.0×10^{-3}
W43 Main (4)	92.2	107.8	98.0	96.8	96.3	4, 6	111.3	7.5	6	4.0×10^{-5}
G31.29+0.07	106.0	109.0	106.0	107.5	107.5	1, 54	108.0	5.6	53	6.5×10^{-5}
G31.25−0.11	14.7	28.3	18.6	20.6	19.3	4, 52, 54	−9.9	15.5	54	3.1×10^{-4}

TABLE 5—*Continued*

Region	$V(H_2O)$ (km s^{-1}) V_{min}[a]	V_{max}[b]	V_m[c]	V_a[d]	V_c[e]	References	V_0[f] (km s^{-1})	D (kpc)	References	$L(H_2O)$[g] ($L_\odot$)
G32.15+0.13	89.6	92.8	92.5	92.1	92.2	1, 4	94.1	7.2	34	2.0×10^{-5}
G32.04+0.06	92.2	96.8	95.3	94.7	94.5	4, 54	95.4	8.5	53	2.3×10^{-4}
G32.10−0.08	46.0	46.0	46.0	46.0	46.0	54	47.9	...		...
G32.74−0.08	32.7	37.7	32.9	34.1	33.1	4, 52, 54	38.2	...		...
G33.91+0.11	109.0	109.0	109.0	109.0	109.0	6	107.0	9.0	6	7.0×10^{-6}
W44	32.0	81.7	54.1	58.1	59.7	4, 6, 55	57.8	3.7	53	8.6×10^{-4}
G35.03+0.3	42.1	70.0	70.0	56.4	64.8	52	52.4	3.6	53	6.6×10^{-5}
S76W	−9.7	6.2	3.5	−2.4	−2.4	2, 4, 12	32.5	2.4	56	1.3×10^{-4}
S76E	24.1	40.7	31.7	31.3	31.1	2, 4, 12	32.9	2.4	56	4.0×10^{-5}
G35.20−0.74	23.5	40.8	36.1	32.9	34.6	4	34.0	2.3	57	2.4×10^{-5}
W48	43.5	46.4	46.0	45.3	45.3	4, 6, 55	42.8	3.0	34	6.4×10^{-6}
G40.62−0.14	34.6	34.6	34.6	34.6	34.6	55	33.8	...		...
G45.49+0.13	60.9	64.0	63.0	62.6	62.7	1	60.8	6.0	34	3.3×10^{-5}
G45.44+0.07	56.0	58.0	56.0	57.0	57.0	4, 6, 52	58.0	6.0	34	5.8×10^{-6}
W51 Main/S	−30.0	170.0	62.5	73.8	68.9	4, 6, 58	55.8	7.0	58	2.0×10^{-2}
S87	11.0	25.5	25.5	19.8	24.4	2, 12	23.3	2.3	59	1.8×10^{-6}
K3-50	−43.6	−11.0	−19.4	−23.6	−23.0	4, 6	−2.0	5.7	34	1.8×10^{-5}
ON 3	−21.4	−18.1	−21.4	−19.8	−20.2	6	−22.6	7.8	34	8.4×10^{-6}
ON 1	−74.9	23.4	13.1	0.6	7.5	4, 6, 44, 60	11.1	3.0	34	1.8×10^{-4}
ON 2S	−11.6	3.2	2.6	−8.3	−3.3	4, 6, 60	−1.2	4.0	34	6.1×10^{-5}
ON 2	−47.1	9.9	5.9	0.9	1.9	4, 6, 44, 60	−0.4	3.9	34	6.1×10^{-4}
S106	−4.4	−1.1	−4.0	−2.6	−2.9	8, 24	−1.0	0.6	61	9.3×10^{-7}
W75N OH	−3.4	25.4	21.1	14.8	16.7	4, 6, 62	9.5	2.0	63	4.4×10^{-5}
W75S (1)	−8.0	4.5	4.5	−1.9	−0.2	4, 6, 44	−3.5	2.0	63	1.4×10^{-5}
W75S (2A+2B)	−14.2	7.3	0.9	−2.9	−2.8	4, 6, 44	−3.3	2.0	63	4.4×10^{-5}
DR 21S	−6.0	−6.0	−6.0	−6.0	−6.0	6	−2.5	2.0	63	2.7×10^{-6}
W75S (3)	−37.9	0.6	−1.3	−8.2	−7.6	4, 6	−3.9	2.0	63	1.2×10^{-5}
NGC 7129 (1)	−13.9	38.2	−9.4	3.2	3.1	4, 8, 23, 25	−9.9	1.1	34	3.3×10^{-7}
NGC 7129 (2)	−46.5	33.6	−8.3	−6.9	−6.5	4, 8, 23, 25, 64	−10.1	1.1	34	2.9×10^{-6}
HHL 73	−2.0	−2.0	−2.0	−2.0	−2.0	42	3.8	0.9	42	2.0×10^{-7}
S140	−16.0	12.3	−15.5	−1.5	−4.4	1, 4, 8, 11	−7.1	0.8	65	7.0×10^{-6}
GGD 37	−32.2	13.9	−8.4	−6.9	−9.4	4, 23, 32, 40	−10.5	0.7	66	5.0×10^{-5}
NGC 7538S	113.3	−43.4	−61.6	−61.4	−58.4	4, 6, 37, 44, 60	−56.4	2.7	67	1.2×10^{-4}
NGC 7538 IR	−81.8	−46.2	−61.8	−59.1	−60.1	4, 6, 60	−56.5	2.7	67	1.2×10^{-4}
S157	−46.0	−43.6	−46.0	−45.3	−45.2	4, 6	−43.4	2.5	5	4.0×10^{-6}

[a] Minimum of the velocity range over which the H_2O maser emission extends.
[b] Maximum of the velocity range over which the H_2O maser emission extends.
[c] Velocity of the absolute maximum of the spectra.
[d] Average of the mean velocities of the components of each spectrum.
[e] Velocity centroid of the maser emission.
[f] Velocity of the high-density gas, taken as the average of the velocities of the CS and NH_3 emission.
[g] Maximum luminosity reported.

References.—(1) Genzel & Downes 1979; (2) Blair et al. 1980; (3) Elmegreen & Lada 1978; (4) Comoretto et al. 1990; (5) Georgelin 1975; (6) Genzel & Downes 1977; (7) Harris & Wynn-Williams 1976; (8) Cesarsky et al. 1978; (9) Anglada et al. 1989; (10) Herbig & Jones 1983; (11) Rodríguez & Cantó 1983; (12) Henkel et al. 1986; (13) Simon et al. 1983; (14) Haschick et al. 1980; (15) Strom et al. 1974; (16) Verdes-Montenegro et al. 1989; (17) Snell et al. 1988; (18) Genzel et al. 1981b; (19) Morris & Knapp 1976; (20) Haschick et al. 1983; (21) Lo et al. 1975; (22) Cohen & Schwartz 1979; (23) Rodríguez et al. 1980; (24) Blair et al. 1978; (25) Sandell & Oloffson 1981; (26) Schwartz & Buhl 1975; (27) Pankonin et al. 1977; (28) Campbell 1978; (29) Downes et al. 1975; (30) Racine 1968; (31) Lada & Wooden 1979; (32) Lada et al. 1981; (33) Batchelor et al. 1980; (34) This paper; (35) Rodríguez et al. 1978; (36) Racine & van den Bergh 1970; (37) White & Macdonald 1979; (38) Moffat et al. 1979; (39) Walker 1956; (40) Blitz & Lada 1979; (41) Crocker & Hagen 1983; (42) Gyulbudaghian et al. 1987; (43) Caswell et al. 1983a; (44) Cato et al. 1976; (45) Gómez et al. 1991; (46) Downes et al. 1980; (47) Fazio et al. 1978; (48) Caswell et al. 1975; (49) Jaffe et al. 1981; (50) Jaffe et al. 1982; (51) Yngvesson et al. 1975; (52) Caswell et al. 1983b; (53) Solomon et al. 1987; (54) Matthews et al. 1985; (55) Evans et al. 1979; (56) Forbes 1989; (57) Little et al. 1983; (58) Genzel et al. 1981a; (59) Fich & Blitz 1984; (60) Forster et al. 1978; (61) Staude et al. 1982; (62) Johnston et al. 1973; (63) Dickel et al. 1969; (64) Wouterloot et al. 1988; (65) Crampton & Fisher 1974; (66) Blaauw et al. 1959; (67) IAU Trans. 1964.

velocities, i.e., the velocity centroid, $V_c(H_2O)$. It must be noted that this determination of the velocity centroid of the maser emission, $V_c(H_2O)$, is independent of the calibration of the different telescopes used in taking the spectra. In addition, for a more direct comparison, we also give in Table 5 the velocity of the high-density gas, V_0, derived from our CS and NH_3 observations.

An estimate of the distance to each source is also given in Table 5. For sources with unknown distance or with an available kinematic distance determined from the H_2O maser velocity, we obtained the kinematic distances from the velocity V_0 of the high-density gas, using the Galactic rotation curve of Fich, Blitz, & Stark (1989). We give this distance in the cases in which there is no twofold distance ambiguity or in which the ambiguity has been resolved. No distance estimate could be obtained for nine of our sources.

Finally, we also give in Table 5 the isotropic luminosity of the maser emission, $L(H_2O)$. For each spectrum the luminosity can be obtained from

$$\left[\frac{L(H_2O)}{L_\odot}\right] = 2.30 \times 10^{-8}\left[\frac{\int S_V\, dV}{\text{Jy km s}^{-1}}\right]\left[\frac{D}{\text{kpc}}\right]^2, \quad (3)$$

where D is the distance to the source, and the integral of the observed flux density extends over all the components of the spectrum. For those cases in which this integral was not

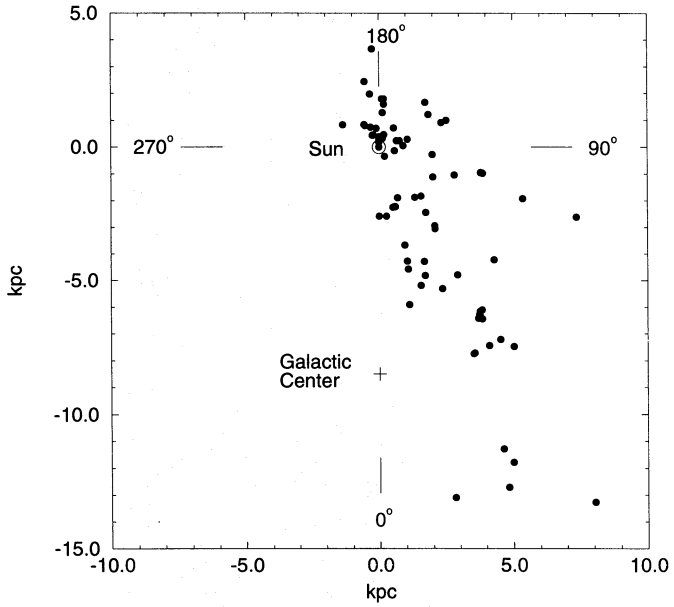

FIG. 7.—Distribution in the Galactic plane of the H_2O maser sources, with estimated distance, that were detected in CS or NH_3. The symbols ⊙ and + indicate the position of the Sun and the Galactic center, respectively.

given in the literature, we estimated it from the published spectra. The luminosities given in the table, for 96 of the 106 sources in which we detected CS or NH_3, correspond to the maximum luminosity reported.

The sources of our sample cover a wide range of distances, as can be seen both in the plot of their positions projected onto the Galactic plane (Fig. 7) and in a histogram of the distances (Fig. 8). In Figure 7 it can be seen as well that our sample is distributed over a significant portion of the Galactic plane that is visible from the northern hemisphere. Thus, our sample appears to be representative of the masers of the Galaxy.

Figure 9*a* shows the distribution of the luminosity of the H_2O masers of our sample (Table 5). This histogram shows a symmetrical distribution centered on $L(H_2O) = 2 \times 10^{-5}$ $L_\odot$ and with luminosities that range from $\sim 10^{-8}$ $L_\odot$ up to $\sim 10^{-2}$ $L_\odot$. From this distribution one could conclude that the typical luminosity of Galactic H_2O masers is $\gtrsim 10^{-5}$ $L_\odot$. Nevertheless, the plot of the maser luminosity versus the distance to the source (Fig. 10), suggests that the selection effects may lead to erroneous conclusions. As can be seen in this figure, the number of low-luminosity masers lowers as the distance increases, which indicates that our sample is limited by instrumental sensitivity. In Figure 9*b*

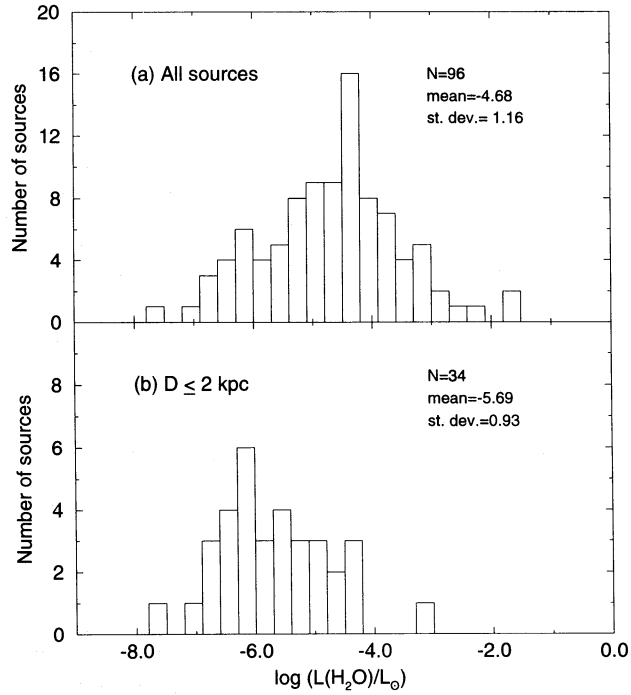

FIG. 9.—Distribution of the luminosity of the H_2O masers that were detected in CS or NH_3. (*a*) All the sources; (*b*) sources with $D \leq 2$ kpc. We also give in the figure the statistical parameters of the distributions.

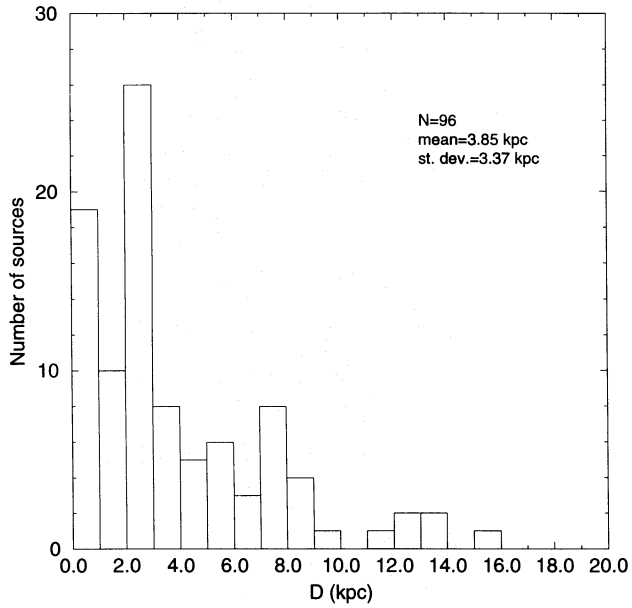

FIG. 8.—Distribution of the distance for H_2O maser sources that were detected in CS or NH_3. We also give in the figure the statistical parameters of the distribution.

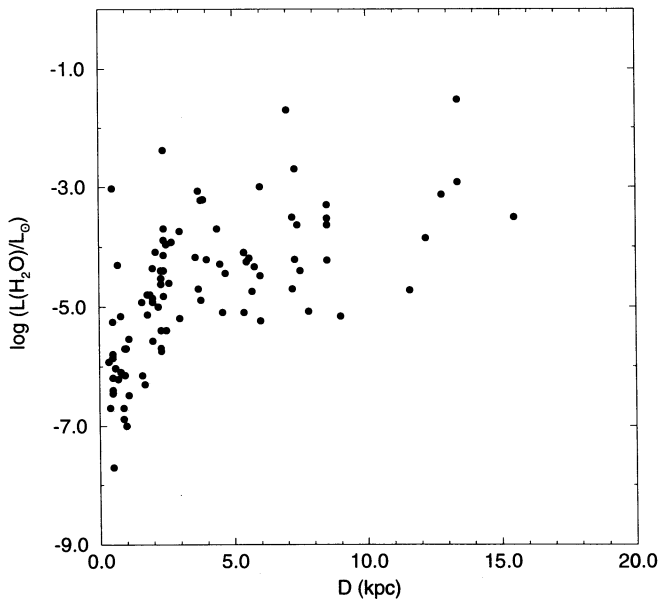

FIG. 10.—Plot of the luminosity of the H_2O masers that were detected in CS or NH_3 vs. the distance to the source.

we plotted the distribution of the nearby masers, with distances smaller than 2 kpc. This distribution appears to be complete down to $L(H_2O) \simeq 10^{-7}\ L_\odot$ and is centered on $L(H_2O) = 2 \times 10^{-6}\ L_\odot$. The comparison of Figure 9*a* with Figure 9*b* makes clear the lack of low-luminosity masers in the former, so that it seems that high-luminosity masers are overabundant in our sample (Table 5) because of selection effects. Consequently, a less biased estimate of the typical luminosity of Galactic H_2O masers seems to be $\sim 10^{-6}\ L_\odot$.

In Figure 11 we show a histogram of the velocity range over which the H_2O maser emission extends, i.e., $V_{max}(H_2O) - V_{min}(H_2O)$. As can be seen in this figure, our sample contains a great variety of H_2O maser spectra, from simple up to very complex ones (e.g., W51 Main/S, whose components extend over ~ 200 km s^{-1}). However, most of the masers, 85% of the sample, do not have very high velocity components, and their velocity ranges are $\lesssim 40$ km s^{-1}.

In Figure 12 we plotted the maser velocity range versus the maser luminosity. From this figure it is clear that the only masers that exhibit a very extended velocity range are the highly luminous ones, whereas the low-luminosity masers do not exhibit high-velocity components. Reid & Moran (1988) note that since H_2O maser emission appears to originate in outflowing condensations, the most likely source for pumping the masers is the kinetic energy dissipated by the small maser condensations as they plow through the ambient molecular cloud. After modeling this interaction, these authors find that the isotropic maser luminosity is expected to be proportional to the cube of the velocity of the maser condensations, $L(H_2O) \propto v^3$. This result is in rough agreement with the trend found in our data, in the sense that only the most luminous masers present a wide range of velocities. Nonetheless, a detailed comparison is not possible from our results since this relationship may be masked by some unavoidable effects. First, selection effects can be important. The intensity of the high-velocity components is usually $\lesssim 10\%$ of the intensity at the maximum. Consequently, the detection of these components strongly depends on the distance to the source and the sensitivity of the observations. So, for a distant low-intensity H_2O maser emission source, its high-velocity components would as a result be undetectable, which would lead to the wrong conclusion that this source does not have any high-velocity component. Second, the observed radial velocity ranges are only lower limits to the real velocities. Thereby, both the selection effects and the projection effects will always tend to decrease the apparent velocity range of the maser emission on the spectrum. Despite these limitations, we can draw the conclusion that masers with high-velocity components are more luminous than masers without high-velocity components.

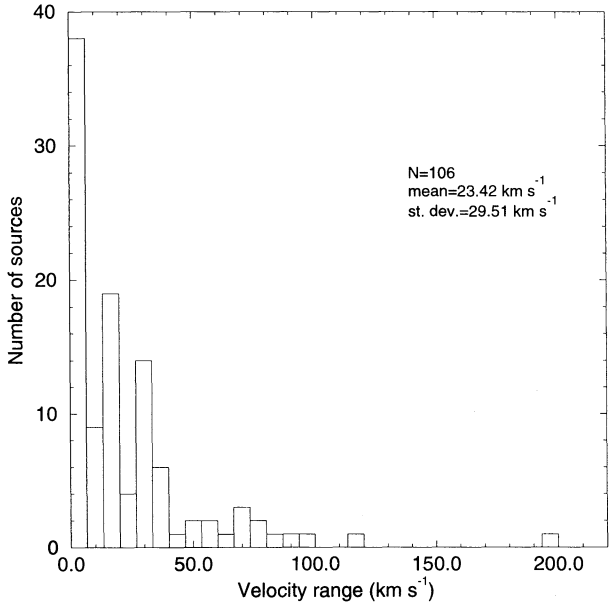

FIG. 11.—Distribution of the range of velocities over which the H_2O maser emission extends, $V_{max}(H_2O) - V_{min}(H_2O)$, for the sources that were detected in CS or NH_3. We also give in the figure the statistical parameters of the distribution.

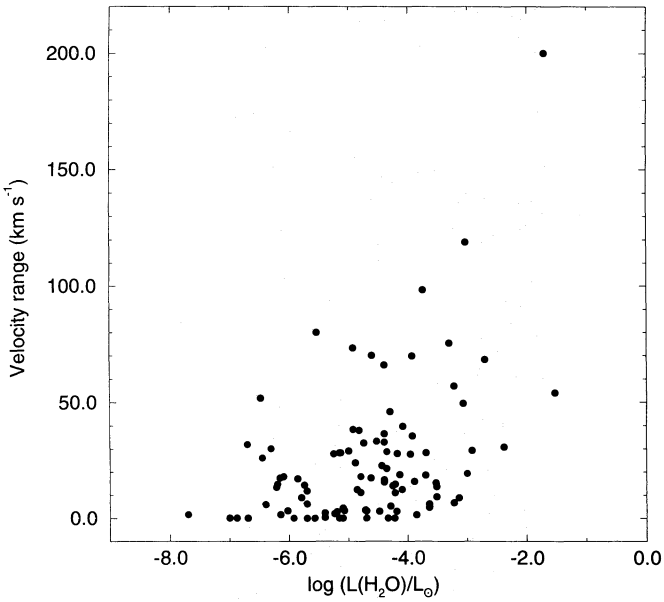

FIG. 12.—Plot of the range of velocities over which the H_2O maser emission extends vs. the maser luminosity for the sources that were detected in CS or NH_3

Figure 13 shows this result more clearly. In Figure 13*b* we present the luminosity distribution of the masers with velocity range <2 km s^{-1}, and in Figure 13*c* we show the same for the masers with velocity range >40 km s^{-1}. The first ones are, on average, ~ 100 times less luminous than the second ones, the luminosity average of each subgroup being $\sim 2 \times 10^{-6}\ L_\odot$ and $\sim 2 \times 10^{-4}\ L_\odot$, respectively. Genzel & Downes (1977) obtained similar conclusions from a study with 69 H_2O maser sources: "single" H_2O masers were ~ 100 times less intense than "complex" masers, the median of their luminosities being $\sim 8 \times 10^{-6}\ L_\odot$ and $\sim 8 \times 10^{-4}\ L_\odot$, respectively. It must be noted here that, although both studies have 44 sources in common, our sample is larger (96 sources), and, in addition, later observations of these sources have been taken into account.

A recent study of the statistical properties and distribution of 88 H_2O masers associated with star forming regions can be found in Palagi et al. (1993).

4.3. *Comparison of the* H_2O *Maser Emission with the* CS *and* NH_3 *Emissions*

In this section we will compare the characteristics of the very small and very dense spots, where the H_2O maser emission originates, with those of the more extended high-density molecular gas, traced by the CS and NH_3 emissions.

First, we will discuss the kinematics of the studied regions

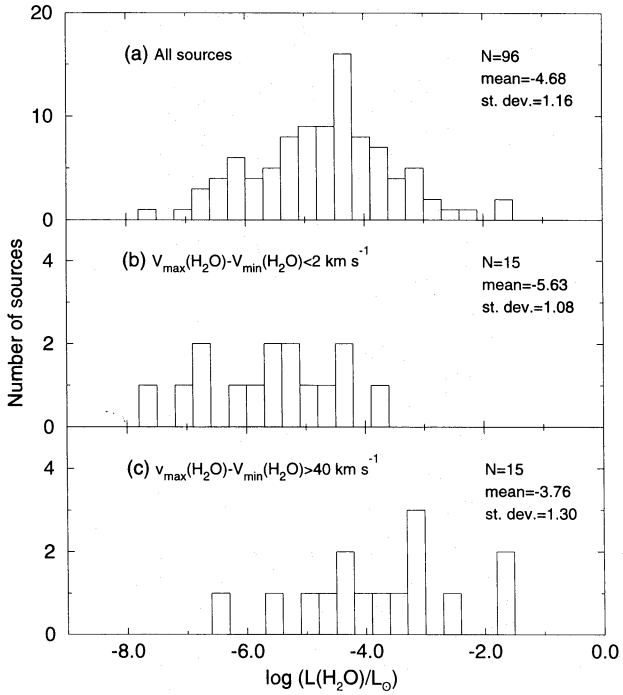

FIG. 13.—Distribution of the luminosity of the H_2O masers that were detected in CS or NH_3. (*a*) All the sources; (*b*) sources with velocity range $V_{max}(H_2O) - V_{min}(H_2O) < 2$ km s^{-1}; (*c*) sources with velocity range $V_{max}(H_2O) - V_{min}(H_2O) > 40$ km s^{-1}. We also give in the figure the statistical parameters of the distributions

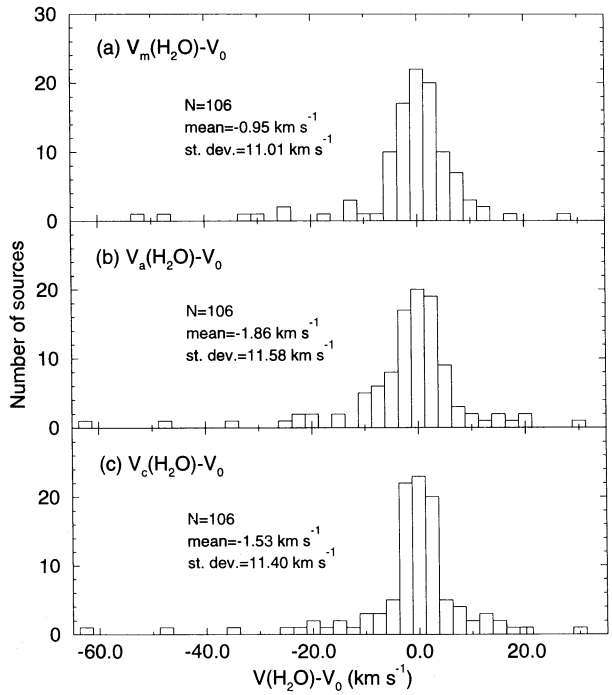

FIG. 14.—Distribution of the difference in velocity between the maser and the high density gas, $V(H_2O) - V_0$. For the velocity of the maser we have adopted: (*a*) the velocity of the maximum $V_m(H_2O)$; (*b*) the average velocity $V_a(H_2O)$; (*c*) the velocity centroid $V_c(H_2O)$ (Table 5). We also give in the figure the statistical parameters of the distributions.

and compare the velocity of the H_2O masers with the velocity of the high-density gas traced by the CS or NH_3 emissions. In Figure 14 we show the histograms of the difference in velocity between the H_2O maser and the high-density gas (see Table 5), taking for the maser the velocity at maximum, $V_m(H_2O)$ (Fig. 14*a*), the average velocity, $V_a(H_2O)$ (Fig. 14*b*), and the velocity centroid, $V_c(H_2O)$ (Fig. 14*c*). These three distributions do not differ significantly, as can be inferred from their statistical parameters: the average is ~ -1 km s^{-1}, the median is ~ 0 km s^{-1}, and the standard deviation ~ 11 km s^{-1}. We obtained a distribution of $V_m(H_2O) - V_0$ very similar to that obtained by Churchwell et al. (1990), although our sample is much larger than the sample they used. For the three distributions the average of $V(H_2O) - V_0$ is negative because of the presence of a few sources with $V(H_2O) \ll V_0$. This asymmetry in the velocity difference distribution is also noted in a sample of 27 H_2O masers detected in CS by Zinchenko et al. (1995), who suggest that this asymmetry could mean that the maser emission is beamed preferably in the direction of its movement relative to its parent cloud.

In fact, in our sample there are six sources (G13.19+0.04, W43 Main (2), G31.25−0.11, S76W, G12.21−0.10, and GGD 29) with $|V(H_2O) - V_0| > 30$ km s^{-1}, the maser velocity being in general the smaller one. On the other hand, in 92% of the sources (98 of 106) the velocity of the cloud either falls inside (70%; 74 out of 106) or at less than 10 km s^{-1} from the velocity range of the maser emission. However, in the regions G13.19+0.04, W43 Main (2), G31.25−0.11, and S76W, the velocity of the cloud is more than 20 km s^{-1} outside the maser velocity range, which is >10 km s^{-1} in all of them. For these particular sources, 4% of our sample, it seems that the molecular and the maser emissions are physically separated, although they appear very close in projection on the sky. This rate agrees with the serendipitous detection rate found by Churchwell et al. (1990), $\sim 5\%$, who used criteria similar to ours in order to sort out these sources. The other two sources with a difference in velocity between the H_2O maser and the molecular cloud >30 km s^{-1} are G12.21−0.10 and GGD 29. G12.21−0.10 is a maser with a very complex spectrum and a large velocity range. The velocity of the cloud falls inside the maser velocity range, although the velocity difference between the H_2O maser (strongest component) and the molecular cloud is ~ 33 km s^{-1}. The case of GGD 29 is similar, but its spectrum is not as complex as for G12.21−0.10. Rodríguez et al. (1980) pointed out that high-velocity H_2O maser emission is often found in the vicinity of the GGD objects, and this causes a shift of the centroid of emission with respect to the velocity of the related dark cloud.

Therefore, despite the wide velocity range over which the H_2O maser emission extends, on average, the characteristic velocity of the maser emission and the velocity of the ambient molecular cloud are very similar. This good agreement suggests a dynamical relationship between the molecular material and the H_2O masers, as has also been suggested by other studies (see, e.g., Churchwell et al. 1990; Torrelles et al. 1992).

In Figure 15 we show the maser luminosity versus the CS and NH_3 line widths (Table 2), corrected for the spectral channel width, for sources detected with a SNR > 5. For both the CS lines (Fig. 15*a*) and the NH_3 lines (Fig. 15*b*), in general, the widest lines are associated with the most luminous H_2O masers. We performed a linear fit to the logarithm of the data. As the uncertainty in the maser luminosity (mainly due to the variability of the maser emission and errors in the distance) is much higher than the error in

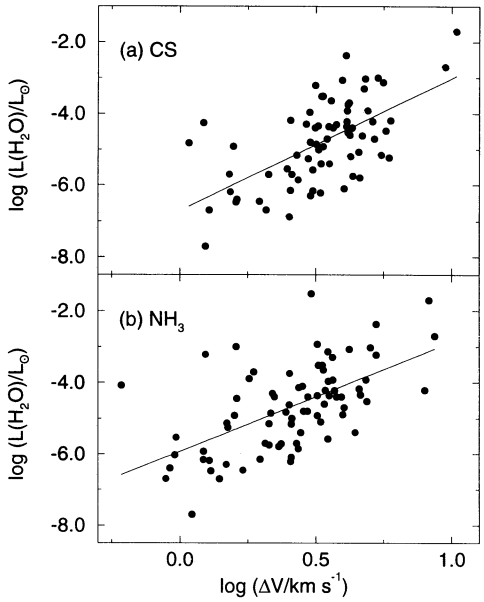

FIG. 15.—Plot of the logarithm of the H_2O maser luminosity vs. the logarithm of the CS (*a*) and NH_3 (*b*) line widths. The straight line is the best linear fit to the data, considering only errors in the vertical axis.

the CS and NH_3 line widths, we considered the line widths as the independent variable in the fit, and we considered errors only in the vertical axis. The fit gives

$$\left[\frac{L(H_2O)}{L_\odot}\right] = 10^{-6.7\pm0.3}\left[\frac{\Delta V(CS)}{\text{km s}^{-1}}\right]^{3.7\pm0.6}, \quad (4)$$

$$\left[\frac{L(H_2O)}{L_\odot}\right] = 10^{-5.9\pm0.2}\left[\frac{\Delta V(NH_3)}{\text{km s}^{-1}}\right]^{3.1\pm0.5}, \quad (5)$$

with a correlation coefficient $r = 0.6$, in both cases.

Therefore, the most luminous masers appear to be associated with a larger perturbation of the molecular gas, as traced by the CS and NH_3 line widths. This result is in agreement with that found in § 4.1.2; that is, regions with H_2O masers present significantly broader CS and NH_3 lines than other regions, which indicates that maser emission is associated with a perturbation of the ambient gas.

Furthermore, in the formulation of Reid & Moran (1988), the maser luminosity is a consequence of the dissipation in the ambient cloud of the kinetic energy of maser condensations associated with outflow motions from a young star, resulting in $L(H_2O) \propto v^3$ (§ 4.2). If the velocity of the maser condensations contributes significantly to the velocity dispersion in the ambient cloud, as measured by the observed line widths, one would expect a similar dependence, $L(H_2O) \propto (\Delta V)^3$, which is consistent with the results of equations (4) and (5). The relationship between luminosity and line width found here is also in agreement with the trend found in § 4.2 between the luminosity and the velocity range of the maser emission.

On the other hand, theoretical models generally require the presence of shocks in order to produce density and temperature suitable for the excitation of H_2O maser emission (see, e.g., Kylafis & Norman 1986; Hollenbach & McKee 1989; Elitzur, Hollenbach, & McKee 1989). For example, Hollenbach & McKee (1989) performed detailed numerical calculations of the structure of a shock wave as it propagates in a relatively high density medium and of the excitation of the H_2O molecule under these conditions. These authors concluded that the resulting physical conditions in the postshock gas (such as those produced by high-velocity outflows from young stellar objects) provide an ideal site for H_2O maser emission. All these results suggest that H_2O maser emission is intrinsically associated with a significant perturbation of the ambient molecular gas, which leads to an increase of the thermal and turbulent energy and results in a broadening of the CS and NH_3 lines.

Churchwell et al. (1990), in a sample of sources associated with H_2O masers, found a weak correlation between the NH_3 line widths and the far-infrared luminosity L_{FIR} (with line width increasing with luminosity). These authors proposed two possible interpretations for this result: first, increasing L_{FIR} is accompanied by increasing mechanical energy input to the ambient molecular cloud via stellar winds; second, more massive (hence, more luminous) stars are formed out of more massive molecular clumps and hence out of regions with larger line widths (from the line width–clump mass relationship).

On the other hand, Wouterloot & Walmsley (1986), Palla et al. (1991, 1993), Henning et al. (1992), Palagi et al. (1993), Codella et al. (1994), and Wilking et al. (1994) found that the H_2O maser luminosity increases with the far-infrared luminosity of the associated *IRAS* sources. Whether or not this correlation represents a real physical relationship is a matter of discussion at the moment.

Therefore, correlations between the maser luminosity, $L(H_2O)$, and the luminosity of the associated *IRAS* source, L_{FIR} (Wouterloot & Walmsley 1986; Palla et al. 1991, 1993; Henning et al. 1992; Palagi et al. 1993; Codella et al. 1994; Wilking et al. 1994), between L_{FIR} and the NH_3 line widths, $\Delta V(NH_3)$ (Churchwell et al. 1990), and between $L(H_2O)$ and the line widths, $\Delta V(CS)$ and $\Delta V(NH_3)$ (this work) have been found recently. Then, our results provide additional physical meaning to the previous two correlations and confirm them independently. These three correlations could naturally be gathered in the following scenario: (1) The infrared source (tracing a young stellar object) is responsible for the excitation, possibly through the energy associated with strong stellar winds, of the maser emission in the small, very high density nearby condensations. (2) These maser condensations are accelerated by the stellar outflow and are seen as high-velocity components in the spectra of some masers. (3) The stellar winds, and also the high-velocity maser condensations, inject mechanical energy and momentum into the surrounding molecular gas, increasing the turbulence and the kinetic temperature, which is observed as an increase in the molecular line widths.

5. CONCLUSIONS

We observed the emissions of the $J = 1 \rightarrow 0$ rotational transition of the CS molecule and the $(J, K) = (1, 1)$ inversion transition of the NH_3 molecule toward 172 star-forming regions associated with H_2O maser emission. We observed 164 sources in NH_3 and 107 in CS. Of these sources, 99 were observed in both molecules. We obtained from the literature the parameters that characterize the H_2O maser emission in those sources that were detected in CS or NH_3. Our main results can be summarized as follows:

1. In the regions that were observed both in CS and in NH_3 the detection rate was very similar, which suggests

that the CS and the NH_3 molecules are excited under similar physical conditions. We detected 106 sources of the 172 that were observed in CS or in NH_3. This high detection rate ($\sim$60%) indicates a remarkable degree of association of the CS and NH_3 emissions with the H_2O maser emission.

2. In general, the observed line widths are larger for the CS than for the NH_3. The CS line widths typically lie between 2 and 5 km s^{-1} ($\sim$72% of the sources), with an average of 3.7 km s^{-1}, while the NH_3 line widths typically lie between 1 and 4 km s^{-1} ($\sim$75% of the sources), with an average of 3.0 km s^{-1}.

3. We found a linear relationship between the CS and NH_3 line widths, $\Delta V(\mathrm{CS}) = 1.1\Delta V(\mathrm{NH_3}) + 0.3$ km s^{-1}. Since the slope is approximately unity, the relationship between the line widths appears to be well described as an additive term confirming previous results (Pastor et al. 1991).

4. The central velocities of the CS and NH_3 lines are very similar, which indicates that both molecules are roughly tracing the same region. Nevertheless, our observations reveal a systematic shift of 0.12 km s^{-1} between the velocities of the CS and NH_3 lines. This shift may have an instrumental origin. The distribution of the difference in velocity between CS and NH_3 has a standard deviation of $\sim$0.6 km s^{-1}, which is quite large as compared with other studies, suggesting that the regions associated with H_2O maser emission present larger velocity inhomogeneities.

5. The luminosity of the studied H_2O masers ranges from $\sim 10^{-8}\ L_\odot$ to $\sim 10^{-2}\ L_\odot$, with an average of $L(\mathrm{H_2O}) = 2 \times 10^{-5}\ L_\odot$. However, for the masers located at distances smaller than 2 kpc, where the selection effects due to the instrumental sensitivity are less important, the mean value of $L(\mathrm{H_2O})$ is $2 \times 10^{-6}\ L_\odot$.

6. We found a relationship between the velocity range over which the H_2O maser emission extends and the luminosity of this emission. Only the masers that exhibit a very extended velocity range are highly luminous, while the low-luminosity masers do not exhibit high-velocity components. The average luminosity is $\sim 2 \times 10^{-4}\ L_\odot$ for the masers with a velocity range >40 km s^{-1} and $\sim 2 \times 10^{-6}\ L_\odot$ for the masers with a velocity range <2 km s^{-1}. This result suggests that the energy source for pumping the masers may be related to the kinetic energy dissipated by the small maser condensations as they move through the ambient molecular cloud.

7. Despite the wide maser velocity range, we found that the characteristic velocity of the maser emission and the velocity of the ambient molecular cloud (traced by the CS and NH_3 emissions) are very similar. The good agreement between these velocities suggests a dynamical relationship between the molecular material and the H_2O masers, as has also been suggested by other studies (Churchwell et al. 1990; Torrelles et al. 1992).

8. We found that the CS and NH_3 lines are significantly wider in regions with an associated H_2O maser than in other regions. Furthermore, we found a correlation between the observed line widths of both the CS and the NH_3 lines and the maser luminosity, with the maser luminosity increasing with the line width. This correlation is consistent with a relation $L(\mathrm{H_2O}) \propto (\Delta V)^3$, in agreement with what is expected if the maser luminosity is a consequence of the dissipation in the ambient cloud of the kinetic energy of outflowing maser condensations. These results suggest that the H_2O maser emission is intrinsically associated with an increase in the thermal and turbulent energy of the ambient cloud; this perturbation of the ambient high-density gas results in a broadening of the observed CS and NH_3 lines. This scenario coincides with that obtained in theoretical models in which the H_2O maser emission originates in a natural way in shocked regions, such as those associated with outflows in young stellar objects.

We thank G. Comoretto for providing us with a computer-readable version of the Arcetri atlas of H_2O masers. We thank G. González-Casado for his help in data analysis at the early stages of this work. We thank an anonymous referee for useful comments. G. A. acknowledges financial support from CIRIT de Catalunya (Spain). G. A. and R. E. are partially supported by DGICYT grant PB92-0900 (Spain). L. F. R. thanks CONACyT and DGAPA-UNAM for financial support.

APPENDIX

ON THE ANTENNA TEMPERATURE RATIO

Let us suppose a lossless antenna working at frequency ν (or wavelength λ), with a Gaussian main beam of FWHM θ_A. The main beam solid angle, Ω_M, is given by

$$\Omega_M = \frac{\pi}{4 \ln 2}\,\theta_A^2 . \tag{A1}$$

The beam efficiency, η_M, and the aperture efficiency, η_A, of the antenna are defined as $\eta_M = \Omega_M/\Omega_A$ and $\eta_A = A_e/(\pi D^2/4)$, where Ω_A is the antenna solid angle (the integral over 4π sr of the antenna power pattern), A_e is the effective aperture of the antenna, $A_e = \lambda^2/\Omega_A$, and D is the antenna diameter. The ratio between the two efficiencies is given by

$$\frac{\eta_M}{\eta_A} = \frac{\pi^2}{16 \ln 2}\left(\frac{D\theta_A}{\lambda}\right)^2 . \tag{A2}$$

If the antenna is diffraction limited, this ratio is essentially independent of the operating wavelength.

Let us consider a small circular radio source, with diameter θ_S or solid angle $\Omega_S = \pi\theta_S^2/4$ and with uniform brightness temperature T_B. The antenna temperature obtained when the antenna points to the center of the source can be easily shown to be

$$T_A^* = \eta_M\, T_B[1 - \exp(-\Omega_S/\Omega_M)] = \eta_M\, T_B[1 - \exp(-\ln 2\ \theta_S^2/\theta_A^2)] . \tag{A3}$$

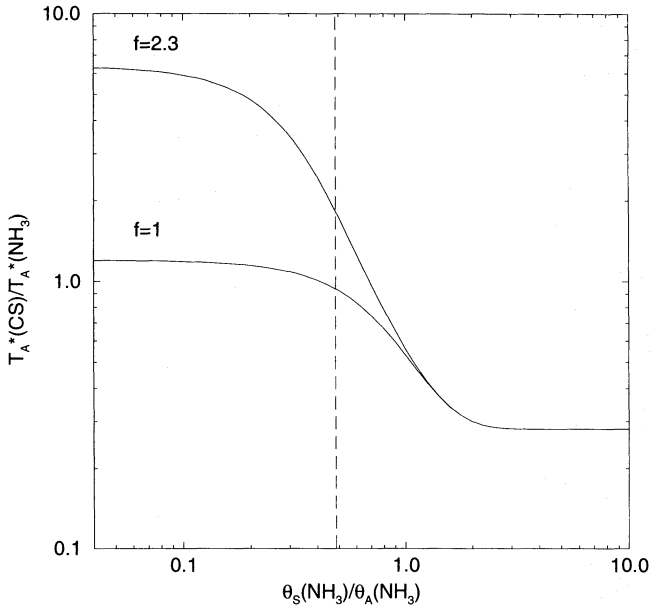

FIG. 16.—Ratio of the antenna temperatures observed with the Haystack antenna at 48.99 GHz (CS $J = 1 \rightarrow 0$) and 23.69 GHz [NH_3 $(J, K) = (1, 1)$] vs. the source diameter at 23.69 GHz measured in units of the half-power beam width of the antenna at 23.69 GHz. For the lower curve the source size is the same at the two frequencies ($f = 1$), while for the upper curve the source size ratio is 2.3 (see text). The vertical dashed line corresponds to a source diameter (at 23.69 GHz) equal to the beam size at 48.99 GHz.

Now, let us consider two different frequencies, ν_1 and ν_2. The size of the source can depend on the frequency, and let f be the ratio of source sizes, $f = \theta_{S2}/\theta_{S1}$. The ratio of the antenna temperatures observed is given by

$$\frac{T_{A2}^*}{T_{A1}^*} = \frac{\eta_{M2}}{\eta_{M1}} \frac{1 - \exp\left(-\ln 2\, \theta_{S2}^2/\theta_{A2}^2\right)}{1 - \exp\left(-\ln 2\, \theta_{S1}^2/\theta_{A1}^2\right)} . \tag{A4}$$

The limit of this ratio for sources unresolved at both frequencies is

$$\lim_{\theta_{S1} \rightarrow 0} \frac{T_{A2}^*}{T_{A1}^*} = f^2 \left(\frac{\Omega_{A2}}{\Omega_{A1}}\right)^{-1} \simeq f^2 \left(\frac{\nu_2}{\nu_1}\right)^2 \frac{\eta_{M2}}{\eta_{M1}} , \tag{A5}$$

while the limit for extended sources is

$$\lim_{\theta_{S1} \rightarrow \infty} \frac{T_{A2}^*}{T_{A1}^*} = \frac{\eta_{M2}}{\eta_{M1}} . \tag{A6}$$

The ratio given by equation (A4) is shown in Figure 16 as a function of source size. The values used for the figure are those of the Haystack antenna for the NH_3 $(J, K) = (1, 1)$ and the CS $(J = 1 \rightarrow 0)$ transitions. That is, $\nu_1 = 23.69$ GHz, $\eta_{M1} = 0.32$, and $\nu_2 = 48.99$ GHz, $\eta_{M2} = 0.09$. For sources of equal size at the two frequencies ($f = 1$), the ratio ranges from 0.28 (source resolved) to 1.2 (source unresolved). If we consider the dependence of source size on frequency, the limit for unresolved sources varies. For $f = 2.3$, i.e., sources 2.3 times larger in CS than in NH_3 (see Pastor et al. 1991), the ratio for unresolved sources is 6.4.

REFERENCES

Anglada, G., Rodríguez, L. F., Torrelles, J. M., Estalella, R., Ho, P. T. P., Cantó, J., López, R., & Verdes-Montenegro, L. 1989, ApJ, 341, 208
Ball, J. 1989, Haystack Obs. Memorandum (Feb. 20)
Ball, J., & Haschick, A. 1988, Haystack Obs. Memorandum (Oct. 12)
Batchelor, R. A., Caswell, J. L., Goss, W. M., Haynes, R. F., Knowles, S. H., & Wellington, K. J. 1980, Australian J. Phys., 33, 139
Benson, P. J., & Myers, P. C. 1989 ApJS, 71, 89
Blaauw, A., Hiltner, N. A., & Johnson, H. L. 1959, ApJ, 130, 69
Blair, G. N., Davis, J. H., & Dickinson, D. F. 1978, ApJ, 226, 435
Blair, G. N., Dinger, A. S. C., & Dickinson, D. F. 1980, AJ, 85, 161
Blitz, L., & Lada, C. J. 1979, ApJ, 227, 152
Brand, J., et al. 1994, A&AS, 103, 541
Braz, M. A., & Epchtein, N. 1983, A&AS, 54, 167
Braz, M. A., Scalise, E., Jr., Gregorio Hetem, J. C., Monteiro do Vale, J. L., & Gaylard, M. 1989, A&AS, 77, 465
Campbell, P. D. 1978, PASP, 90, 262
Caselli, P., & Myers, P. C. 1995, ApJ, 446, 665
Caswell, J. L., Batchelor, R. A., Forster, J. R., & Wellington, K. J. 1983a, Australian J. Phys., 36, 401
———. 1983b, Australian J. Phys., 36, 443
Caswell, J. L., Murray, J. D., Roger, R. S., Cole, D. D., & Cooke, D. J. 1975, A&A, 45, 239
Cato, B. T., Rönnäng, B. O., Rydbeck, O. E. H., Lewin, P. T., Yngvesson, K. S., Cardiasmenos, A. G., & Shanley, J. F. 1976, ApJ, 208, 87
Cesaroni, R., Palagi, F., Felli, M., Catarzi, M., Comoretto, G., Di Franco, S., Giovanardi, C., & Palla, F. 1988, A&AS, 76, 445
Cesarsky, J., Cesarsky, D. A., Churchwell, E., & Lequeux, J. 1978, A&A, 68, 33
Cheung, A. C., Rank, D. M., Townes, C. H., Thornton, D. D., & Welch, W. J. 1969, Nature, 221, 626
Churchwell, E., Walmsley, C. M., & Cesaroni, R. 1990, A&AS, 83, 119
Codella, C., & Felli, M. 1995, A&A, 302, 521
Codella, C., Felli, M., Natale, V., Palagi, F., & Palla, F. 1994, A&A, 291, 261
Codella, C., Palumbo, G. G. C., Pareschi, G., Scappini, F., Caselli, P., & Attolini, R. 1995, MNRAS, 276, 57
Cohen, M., & Schwartz, R. D. 1979, ApJ, 233, L77
Comoretto, G., et al. 1990, A&AS, 84, 179
Crampton, D., & Fisher, W. A. 1974, Publ. Dom. Astrophys. Obs. Victoria, 14, 12
Crocker, D. A., & Hagen, W. 1983, A&AS, 54, 405
Dickel, H. R., Wendker, H., & Bieritz, J. H. 1969, A&A, 1, 270
Dinger, A. S. C., & Dickinson, D. F. 1980, AJ, 85, 1247
Downes, D., Wilson, T. L., Bieging, J., & Wink, J. 1980, A&AS, 40, 379

Downes, D., Winnberg, A., Goss, W. M., & Johansson, L. E. B. 1975, A&A, 44, 243
Elitzur, M., Hollenbach, D. J., & McKee, C. F. 1989, ApJ, 346, 983
Elmegreen, B. G., & Lada, C. J. 1978, ApJ, 219, 467
Evans, N. J., Beckwith, S., Brown, R. L., & Gilmore, W. 1979, ApJ, 227, 450
Fazio, G. C., Lada, C. J., Kleinmann, D. E., Wright, E. L., Ho, P. T. P., & Low, F. J. 1978, ApJ, 221, L77
Felli, M., Palagi, F., & Tofani, G. 1992, A&A, 255, 293
Fich, M., & Blitz, L. 1984, ApJ, 279, 125
Fich, M., Blitz, L., & Stark, A. A. 1989, ApJ, 342, 272
Forbes, D. 1989, A&AS, 77, 439
Forster, J. R., Welch, W. J., & Wright, M. C. H. 1978, ApJ, 221, 137
Genzel, R., & Downes, D. 1977, A&AS, 30, 145
———. 1979, A&A, 72, 234
Genzel, R., et al. 1981a, ApJ, 247, 1039
Genzel, R., Reid, M. J., Moran, J. M., & Downes, D. 1981b, ApJ, 244, 884
Georgelin, Y. 1975, Thèse de Doctorat, Université de Provence
Gómez, Y., Rodríguez, L. F., Garay, G., & Moran, J. M. 1991, ApJ, 377, 519
Gyulbudaghian, A. L., Rodríguez, L. F., & Curiel, S. 1990, Rev. Mexicana Astron. Astrofis., 20, 51
Gyulbudaghian, A. L., Rodríguez, L. F., & Mendoza-Torres, E. 1987, Rev. Mexicana Astron. Astrofis., 15, 53
Harris, S., & Wynn-Williams, C. G. 1976, MNRAS, 174, 649
Haschick, A. D., Moran, J. M., Rodríguez, L. F., Burke, B. F., Greenfield, P., & García-Barreto, J. A. 1980, ApJ, 237, 26
Haschick, A. D., Moran, J. M., Rodríguez, L. F., & Ho, P. T. P. 1983, ApJ, 265, 281
Henkel, C., Haschick, A. D., & Güsten, R. 1986, A&A, 165, 197
Henning, Th., Cesaroni, R., Walmsley, M., & Pfau, W. 1992, A&AS, 93, 525
Herbig, G. H., & Jones, B. F. 1983, A&A, 88, 1040
Ho, P. T. P. 1977, Ph.D. thesis, MIT
Hollenbach, D., & McKee, C. F. 1989, ApJ, 342, 306
IAU Trans. 1964, 12B, 351
Jaffe, D. T., Gusten, R., & Downes, D. 1981, ApJ, 250, 621
Jaffe, D. T., Stier, M. T., & Fazio, G. G. 1982, ApJ, 252, 601
Johnston, K. J., Sloanaker, R. M., & Bologna, J. M. 1973, ApJ, 182, 67
Kylafis, N. D., & Norman 1986, ApJ, 300, L73
Lada, C. J., Blitz, L., & Moran, J. M. 1981, ApJ, 243, 769
Lada, C. J., & Wooden, D. 1979, ApJ, 232, 158
Larson, R. B. 1981, MNRAS, 194, 809
Little, L. T., Brown, A. T., Riley, P. W., Matthews, N., Macdonald, G. H., Vizard, D. R., & Cohen, R. J. 1983, MNRAS, 203, 409
Lo, K. Y., Burke, B. F., & Haschick, A. D. 1975, ApJ, 202, 81
Lovas, F. J. 1986, J. Phys. Chem. Ref. Data, 15, 251
Matthews, H. E., Olnon, F. M., Winnberg, A., & Baud, B. 1985, A&A, 149, 227
Moffat, A. F. J., Fitzgerald, M. P., & Jackson, P. D. 1979, A&AS, 8, 197
Moran, J. M., & Rodríguez, L. F. 1980, ApJ, 236, L159
Morata, O., Estalella, R., López, R., & Planesas, P. 1996, in preparation
Morris, M., & Knapp, G. R. 1976, ApJ, 204, 415
Palagi, F., Cesaroni, R., Comoretto, G., Felli, M., & Natale, V. 1993, A&AS, 101, 153
Palla, F., Brand, J., Cesaroni, R., Comoretto, G., & Felli, M. 1991, A&A, 246, 249
Palla, F., Cesaroni, R., Brand, J., Caselli, P., Comoretto, G., & Felli, M. 1993, A&A, 280, 599
Pankonin, V., Winnberg, A., & Booth, R. S. 1977, A&A, 58, L25
Pastor, J., Estalella, R., López, R., Anglada, G., Planesas, P., & Buj, J. 1991, A&A, 252, 320
Persi, P., Palagi, F., & Felli, M. 1994, A&A, 291, 577
Plume, R., Jaffe, D. T., & Evans, N. J., II. 1992, ApJS, 78, 505
Racine, R. 1968, AJ, 73, 233
Racine, R., & van den Bergh, S. 1970, in IAU Symp. 38, The Spiral Structure of Our Galaxy, ed. W. Becker & G. Contopoulos (Dordrecht: Reidel), 219
Reid, M. J., & Moran, J. M. 1988, in Galactic and Extra Galactic Radio Astronomy, ed. G. L. Verschuur & K. I. Kellermann (New York: Springer), 255
Rodríguez, L. F., & Cantó, J. 1983, Rev. Mexicana Astron. Astrofis., 8, 163
Rodríguez, L. F., Curiel, S., Moran, J. M., Mirabel, I. F., Roth, M., & Garay, G. 1989, ApJ, 346, L85
Rodríguez, L. F., Haschick, A. D., Torrelles, J. M., & Myers, P. C. 1987, A&A, 186, 319
Rodríguez, L. F., Moran, J. M., Dickinson, D. F., & Gyulbudaghian, A. L. 1978, ApJ, 226, 115
Rodríguez, L. F., Moran, J. M., Ho, P. T. P., & Gottlieb, E. W. 1980, ApJ, 235, 845
Sandell, G., & Oloffson, H. 1981, A&A, 99, 80
Scalise, E., Jr., & Monteiro do Vale, J. L. 1987, IAU Circ., 4414
Scalise, E., Jr., Rodríguez, L. F., & Mendoza-Torres, E. 1989, A&A, 221, 105
Schwartz, P. R., & Buhl, D. 1975, ApJ, 201, L27
Simon, M., Felli, M., Cassar, L., Fisher, J., & Massi, M. 1983, ApJ, 266, 623
Snell, R. L., Huang, Y. L., Dickman, R. L., & Claussen, M. J. 1988, ApJ, 325, 853
Solomon, P. M., Rivolo, A. R., Barrett, J., & Yahil, A. 1987, ApJ, 319, 730
Staude, H. J., Lenzen, R., Dyck, H. M., & Schmidt, G. D. 1982, ApJ, 255, 95
Strom S. E., Grasdalen, G. L., & Strom, K. M. 1974, ApJ, 191, 111
Tofani, G., Felli, M., Taylor, G. B., & Hunter, T. R. 1995, A&AS, 112, 299
Torrelles, J. M., Gómez, J. F., Anglada, G., Estalella, R., Mauersberger, R., & Eiroa, C. 1992, ApJ, 392, 616
Torrelles, J. M., Ho, P. T. P., Moran, J. M., Rodríguez, L. F., & Cantó, J. 1986, ApJ, 307, 787
Torrelles, J. M., Ho, P. T. P., Rodríguez, L. F., & Cantó, J. 1990, ApJ, 349, 529
Verdes-Montenegro, L., Torrelles, J. M., Rodríguez, L. F., Anglada, G., López, R., Estalella, R., Cantó, J., & Ho, P. T. P. 1989, ApJ, 346, 193
Walker, M. F. 1956, ApJS, 2, 365
White, G. J., & Macdonald, G. H. 1979, MNRAS, 188, 745
Wilking, B. A., Claussen, M. J., Benson, P. J., Myers, P. C., Tereby, S., & Wootten, A. 1994, ApJ, 431, L119
Wood, D. O. S., & Churchwell, E. 1989, ApJ, 340, 265
Wouterloot, J. G. A., Brand, J., & Henkel, C. 1988, A&A, 191, 323
Wouterloot, J. G. A., & Walmsley, C. M. 1986, A&A, 168, 237
Xiang, D., & Turner, B. E. 1995, ApJS, 99, 121
Yngvesson, K. S., Cardiasmenos, A. G., Shanley, J. F., Rydbeck, O. E. H., & Elldér, J. 1975, ApJ, 195, 91
Zhou, S., Wu, Y., Evans, N. J., Fuller, G. A., & Myers, P. C. 1989, ApJ, 346, 168
Zinchenko, I., Mattila, K., & Toriseva, M. 1995, A&AS, 111, 95